The E3 Ubiquitin Ligase Mind Bomb 1 Controls Adenovirus Genome Release at the Nuclear Pore Complex

Bauer, Michael ; Flatt, Justin W ; Seiler, Daria ; Cardel, Bettina ; Emmenlauer, Mario ; Boucke, Karin ; Suomalainen, Maarit ; Hemmi, Silvio ; Greber, Urs F

Abstract: Adenoviruses (AdVs) cause respiratory, ocular, and gastrointestinal tract infection and inflammation in immunocompetent people and life-threatening disease upon immunosuppression. AdV vectors are widely used in gene therapy and vaccination. Incoming particles attach to nuclear pore complexes (NPCs) of post-mitotic cells, then rupture and deliver viral DNA (vDNA) to the nucleus or misdeliver to the cytosol. Our genome-wide RNAi screen in AdV-infected cells identified the RING-type E3 ubiquitin ligase Mind bomb 1 (Mib1) as a proviral host factor for AdV infection. Mib1 is implicated in Notch-Delta signaling, ciliary biogenesis, and RNA innate immunity. Mib1 depletion arrested incoming AdVs at NPCs. Induced expression of full-length but not ligase-defective Mib1 in knockout cells triggered vDNA uncoating from NPC-tethered virions, nuclear import, misdelivery of vDNA, and vDNA expression. Mib1 is an essential host factor for AdV uncoating in human cells, and it provides a new concept for licensing virion DNA delivery through the NPC.

DOI: https://doi.org/10.1016/j.celrep.2019.11.064

The E3 Ubiquitin Ligase Mind Bomb 1 Controls Adenovirus Genome Release at the Nuclear Pore Complex

Michael Bauer,[1,2] Justin W. Flatt,[1,3] Daria Seiler,[1] Bettina Cardel,[1] Mario Emmenlauer,[4] Karin Boucke,[1] Maarit Suomalainen,[1] Silvio Hemmi,[1] Urs F. Greber [1,*]

[1] Department of Molecular Life Sciences, University of Zurich, 8057 Zurich, Switzerland.

[2] Life Science Zurich Graduate School, ETH and University of Zurich, 8057 Zurich, Switzerland.

[3] Institute of Biotechnology & Department of Biosciences, University of Helsinki, 00790 Helsinki, Finland

[4] BioDataAnalysis GmbH, Balanstrasse 43, 81669 Munich, Germany

* Correspondence & lead contact: urs.greber@imls.uzh.ch

Telephone: +41 44 635 4841, Fax: +41 44 635 6817

Summary

Adenoviruses (AdVs) cause respiratory, ocular and gastro-intestinal tract infections and inflammations in immuno-competent people, and life-threatening disease upon immuno-suppression. AdV vectors are widely used in gene therapy and vaccination. Incoming particles attach to nuclear pore complexes (NPCs) of post-mitotic cells, rupture, and deliver viral DNA (vDNA) to the nucleus and misdeliver to the cytosol. Our genome-wide RNA-interference screen in AdV infected cells identified the RING-type E3-ubiquitin ligase Mind bomb 1 (Mib1) as a proviral host factor for AdV infection. Mib1 is implicated in Notch/Delta signalling, ciliary biogenesis, and RNA innate immunity. Mib1 depletion arrested incoming AdVs at NPCs. Induced expression of full-length but not ligase-defective Mib1 in knockout cells triggered the vDNA uncoating from NPC-tethered virions, nuclear import, misdelivery of vDNA, and vDNA expression. Mib1 is an essential host factor for AdV uncoating in human cells, and provides a new concept for licensing virion DNA delivery through the NPC.

Highlights

- Genome-wide RNAi screen identifies host factors boosting or inhibiting AdV entry

- The E3 ubiquitin ligase Mib1 enhances the entry of AdV from different species

- Ubiquitination activity of Mib1 licenses AdV uncoating at the nuclear pore complex

- Mib1 at NPC-docked AdV releases viral DNA into nucleus and cytosol ‘on demand’

eTOC blurb

Adenoviruses infect multiple organs in humans, delivering their DNA genome for replication to the nucleus. Adenovirus vectors are widely used in clinics. Bauer et al. identify a novel mechanism for virion-DNA uncoating at the nuclear pore complex, licenced by the E3 ubiquitin ligase activity of Mind bomb 1.

Introduction

Molecular interactions in virus infected cells control the outcome of infection. Signalling events from the virus particle, virion to the cell affect for example nutrient sensing pathways, cell cycle progression, growth, migration, anti-viral immunity, cell survival and death. In turn, virions receive chemical and mechanical cues from the invaded cell, and thereupon engage a controlled, stepwise destabilization process, which culminates in the uncoating of the genome (Wolfrum and Greber, 2013; Yamauchi and Greber, 2016). In most cases, the dismantling starts upon receptor binding at the plasma membrane, and continues in endosomes, the cytoplasm and the nucleus until the genome is completely uncoated (Flatt and Greber, 2017; Marsh and Helenius, 2006; Wang et al., 2018; Witte et al., 2018).

Viruses deliver their genome into the nucleus of post-mitotic cells by hijacking the nuclear import machinery and the nuclear pore complex (NPC). The NPC provides a size-limited passageway between the cytoplasm and the nucleoplasm (Kim et al., 2018; Schmidt and Gorlich, 2016). It restricts the import of most viral capsids, with the exception of very small capsids, such as parvoviruses and circoviruses (Kobiler et al., 2012). Hepatitis B virus with a similarly small capsid is thought to enter the NPC and dissociate its closed circular and partly double-stranded DNA within the NPC by a spring-loaded mechanism (Dhason et al., 2012). Virion mechanics are implicated in releasing the pressurized DNA genome from herpesvirus capsids, and also entropically confined genomes in adenovirus (AdV) particles at the NPC (Greber, 2016; Shahin et al., 2006).

AdVs are widespread and cause a variety of infections in vertebrates, including fish, repitiles, rodents, birds, non-human primates and humans (Davison et al., 2003). Human AdVs infect the respiratory and gastrointestinal tracts, the kidney, liver, eye as well as blood cells, and persist in lymphoid cells of the digestive tract, and can cause inflammatory disease (Cook and Radke, 2017). The human AdV species C type 2 or 5 (AdV-C2/5) particles enclose a linear double-stranded DNA of ~36 kbp in an icosahedral capsid of ~90 nm. In the stepwise entry process, they shed the fibers and pentons, expose the membrane lytic protein VI, rupture the endosome and engage in cytoplasmic transport to the nuclear envelope docking to the NPC and releasing the genome for nuclear import along with protein VII, which is assembled with the vDNA in a nucleosome-like structure

(Burckhardt et al., 2011; Cassany et al., 2015; Greber et al., 1993; Luisoni et al., 2015; Moyer et al., 2011; Ostapchuk et al., 2017; Trotman et al., 2001; Wang et al., 2017; Wiethoff et al., 2005). The partly dismantled virions rupture at the NPC by mechanical force from microtubule-dependent motors (Strunze et al., 2011), and release the genome to the nucleus for transcription, but also misdeliver vDNA to the cytosol (Puntener et al., 2011; Wang et al., 2013). Misdelivered DNA is decoded by cytosolic DNA sensors, such as cGAS and the inflammasome (Lam et al., 2014), which explains at least in part the inflammatory nature of AdV infections in a broad range of cell types, including immune cells (Greber and Flatt, 2019). The intricate entry process involves a plethora of host factors, most of which are unknown. Here, we conducted a genome-wide RNA-interference screen in human cells infected with AdV-C2. We identified a novel licensing factor for viral genome uncoating at the NPC, the E3-ubiquitin ligase Mind bomb 1 (Mib1), and show that the ligase activity controls the nuclear import and cytoplasmic misdelivery of vDNA from AdV-C2/5.

Results and Discussion

Genome-wide RNA interference against AdV infection

In search for new host factors involved in AdV entry and gene expression, we performed an arrayed genome-wide, image-based small interfering (si) RNA screen using four siRNAs combined per gene in HeLa cells. Dissecting molecular functions of cells by RNA interference (RNAi) screens is a powerful yet inherently noisy procedure with off-target effects due to cell toxicity of the siRNAs or their functioning as microRNAs with a broad range of targets (Daga et al., 2018; Franceschini et al., 2014). Genome-wide RNAi screens were reported for a range of viruses, including human immune deficiency virus, hepatitis C virus, Ebola virus, West Nile virus, vaccinia virus, influenza A virus, papillomavirus, enterovirus 71, bunyavirus, Semliki Forest virus, rotavirus and adeno-associated virus, but not AdV (Balistreri et al., 2014; Goff, 2008; Green and Pelkmans, 2016; Hao et al., 2013; Karlas et al., 2010; Krishnan et al., 2008; Li et al., 2009; Lipovsky et al., 2013; Mano et al., 2015; Meier et al., 2014; Smith et al., 2010; Su et al., 2013; Watanabe et al., 2010; Wu et al., 2016).

Here we provide the first genome-wide RNAi screen for AdV. Cells were infected with AdV-C2 encoding GFP under a CMV promoter in place of the E3B gene region (AdV-C2-ΔE3B-CMV-GFP) at a multiplicity of infection (MOI) of 0.1 (Yakimovich et al., 2012), stained with DAPI and phalloidin to label the cytoplasmic F-actin, imaged in a high-throughput microscope, and analyzed for GFP expression 16 h post infection (pi) (Fig. 1A). The procedure was similar to a previous siRNA screen of the human kinome with a range of pathogens, including AdV-C2-dE3B-GFP (Ramo et al., 2014). Z-score analyses of 16'462 host genes indicated a continuous distribution of hits, where 159 siRNA pools gave Z scores smaller than -2 (inhibiting infection) and 440 larger than +2 (enhancing infection) in an overall range from -2.99 to +6.51 (Fig. 1B, and Supplemental Table 1). The top 500 siRNAs downregulating infection gave Z-scores < -1.57 (Supplemental Table 2). Grouping these hits into functional clusters using STRING (Szklarczyk et al., 2017) gave low false discovery rates smaller than 10^{-4} in case of the COP-I coated vesicle machinery, NPC components, the mediator complex, spliceosomal complex, cytosolic ribosomes, preribosomes, or the nucleolus, which are directly or indirectly involved in gene expression and protein production (Supplemental Fig. 1A) (Berk, 2005; Vijayalingam and Chinnadurai, 2013). The top 500 siRNAs upregulating infection had Z-scores > +1.91 (Supplemental Table 3), and comprised broadly defined clusters, such as endo-lysosomal membranes, intracellular organelles, or protein-protein complexes with high false discovery rates between 0.01 and 0.05. These hits may reflect the fact that HeLa cells have compromised anti-viral defense, for example due to expression of the human papilloma virus E6 and E7 proteins, which antagonize p53, pRb, or cyclic GMP-AMP synthase (see Supplemental Fig. 1B, and Lau et al., 2015; Mantovani and Banks, 2001; Munger et al., 2001).

The E3 Ub ligase Mib1 controlling developmental signalling and innate immunity is broadly required for AdV infection

We analyzed siRNA hits downregulating AdV infection, particularly those not affecting host gene expression and protein synthesis, and focussed on one of the strongest hits in our validation, the E3 ubiquitin (Ub) ligase Mib1. Mib1 is a RING (really interesting new gene)-type E3 Ub ligase of 1006 amino acids, first discovered in Zebrafish and highly conserved in almost all higher organisms (Deshaies and Joazeiro, 2009). It localizes to centriolar satellite complexes on microtubules in the vicinity of the centrosome (Villumsen et al., 2013). Ubiquitination can have a strong impact on the structure, function, localization, and

stability of the targeted protein, and viruses have evolved to exploit ubiquitination (Komander and Rape, 2012; Luo, 2016). For example, the Ub-proteasome system has been implicated in entry of dengue virus, Kaposi's sarcoma-associated herpesvirus, vaccinia virus and influenza virus (Banerjee et al., 2014; Dejarnac et al., 2018; Greene et al., 2012; Gschweitl et al., 2016; Mercer et al., 2012; Su et al., 2013). Human AdVs have also been shown to manipulate the cellular ubiquitination machinery during replication (Orazio et al., 2011; Querido et al., 2001; Schreiner et al., 2010). Yet, a role for a specific E3 Ub ligase in virion dismantling has remained elusive.

Our RNA interference against the E3 Ub ligase Mib1 strongly reduced AdV infection but not cell numbers, with infection and cell number Z-scores of -2.15 and +0.54, respectively (Supplemental Table 1). Four different siRNAs for Mib1 independently depleted the Mib1 protein levels and reduced the infection of HeLa, diploid human WI-38 fibroblasts and human epithelial lung carcinoma A549 cells with AdV-C5-E1A-FS2A-GFP (AdV-C5-GFP), whereas non-targeting control siRNAs (siNT) had no effect (Fig. 1C-E). AdV-C5-GFP expressed stand-alone GFP from the immediate early viral E1A-GFP hybrid mRNA with a 'ribosome-skipping' F2A sequence (Minskaia et al., 2013), placed between the E1A and GFP open reading frames. We observed strong infection inhibition and loss of Mib1 in polyclonal CRISPR/Cas9 Mib1 knock-out (KO) HeLa and A549 cells edited with a guide RNA directed to the first Mib1 exon, but not a non-targeting control guide RNA (sgNT) (Supplemental Fig. 1C-D). The dramatic block of AdV-C5 infection was confirmed in a monoclonal HeLa-sgMib1 line (clone 1), which had an insertion of a thymidine at position 62 in all the Mib1 alleles. The HeLa-ATCC cells have three Mib1 genes (Adey et al., 2013). The insertion of a thymidine gave rise to a translational stop codon TGA, 186 nucleotides downstream of the insertion, and complete resistance to AdV-C5 infection, as indicated by the lack of the immediate early viral protein E1A (Supplemental Fig. 1E-F). Clone 1 was also resistant to AdV species A, B and D, but remained susceptible to herpes simplex virus 1 (HSV-1), pseudotyped lentivirus, vesicular stomatitis virus (VSV), and influenza A virus (IAV) infections (Fig. 1F, Supplemental Fig. 1G). Mib1 KO cells even enhanced the infection with the RNA viruses IAV and VSV, possibly due to reduced anti-viral activity in Mib1 KO cells (Li et al., 2011). Regardless, the ectopic expression of Mib1 by a lentivirus in the Mib1-KO cells completely restored both AdV-C5 infection and Mib1 expression (Fig. 1G-H).

Loss of Mib1 arrests incoming AdV at the NPC and blocks vDNA uncoating

AdV enters cells by receptor mediated endocytosis, followed by penetration of the endosome, cytoplasmic transport, docking to the NPC and release of the genome into the nucleus (Fig. 2A, and Greber and Flatt, 2019). Microscopic analyses of single virions in single cells showed no reduction in AdV-C5 binding or endocytosis into cells treated with Mib1 siRNA or siNT, nor the exposure of the membrane lytic protein VI, or nuclear targeting (Fig. 2B-E, Supplemental Fig. 2A-D). Remarkably though, sgMib1 cells appeared to contain more virions at the nucleus 5 and 8 h pi, suggesting that Mib1 was involved in turning over intracellular AdV particles. During AdV uncoating in unperturbed cells, AdV capsid fragments are displaced from the NPC to the cell periphery (Strunze et al., 2011). Electron microscopy up to 7 h pi indicated no reduction of incoming AdV-C5 at the nuclear membrane in sgMib1 cells, unlike control cells, which showed a strong decline in virions compared to 1 h pi (Fig. 3A-B). This suggested a stable interaction of virions with NPCs in the absence of Mib1. This notion was supported by the finding that in Mib1-depleted cells, more virions colocalized with NPCs 8 h pi than in control cells, as indicated by single section super-resolution STED microscopy (Supplemental Fig. 3A-C). It is of note that several capsid puncta did not perfectly colocalize with the anti-NPC antibody Mab414, which reacts with the central transporter protein p62, the cytoplasmic filaments and the nuclear basket structures (Walther et al., 2001). Imperfect colocalization of AdV with Mab414 may reflect a heterogeneity of virion docking at NPCs (Cassany et al., 2015; Strunze et al., 2011; Trotman et al., 2001), or local curvature of the nuclear membrane. The latter gives rise to lateral rather than ‘on face’ views of AdV-NPC contacts, a phenomenon, which is observed in the superresolved confocal images at the nuclear edge (Supplemental Fig. 3A). Regardless, our analyses of single confocal mid-sections unequivocally showed strong colocalization of viral DNA with the capsids at the nuclear membrane of sgMib1 cells, and no evidence of vDNA in the nucleus, unlike control cells showing capsid-free viral genomes inside the nucleus, as delimited by lamin staining (Supplemental Fig. 3D).

Next, we probed the genome contents of these particles using click chemistry, N_3-AlexaFluor 488 and confocal microscopy. Analyses of thousands of 5-ethynyl-2’-deoxycytidine (EdC)-labeled viral genomes confirmed the virtual absence of vDNA separation from the capsids up to 5.5 h pi (Fig. 3C). Maximum image projections showed

that nearly all the virions of control cells released their genome either into the nucleus or misdelivered it to the cytosol (Fig. 3D). Mib1 depleted cells, however, showed almost no free viral genomes in the nucleus or the cytoplasm, but contained abundant amounts of EdC genome-positive virions, stained by the azide-containing fluorophore probe and contained in the leaky capsid. Such capsids are partly dismantled particles (Wang et al., 2013), and were readily detected in the cytosol of both control and Mib1-lacking cells 30 min pi (Fig. 3C-D). The data demonstrate that the release of vDNA from capsid and vDNA nuclear import are dramatically impaired in the absence of Mib1.

The Ub ligase activity of Mib1 is required to reverse the AdV uncoating defect

Mib1 is an E3 Ub ligase with three main domains, an N-terminal region comprising Mib-Herc2 domains with a ZZ zinc finger, a middle region containing nine ankyrin repeats, and a C-terminal region containing three RING domains (Fig. 4A). While the N-terminal region mediates protein-protein interactions (Mertz et al., 2015), the C-terminal RING domain has E3 Ub ligase activity. We expressed various flag-tagged truncation mutants as well as two point mutants of Mib1 in sgMib1 cells by lentiviral transduction. While AdV-C5-GFP infection was completely restored by expression of full length Mib1, none of the truncation mutants rescued the infection, suggesting that both the N-terminal and C-terminal domains are required for AdV infection (Fig. 4B-C). Expression of a full length serine 805 to alanine (S805A) mutant abrogating phosphorylation at this position (Berndt et al., 2011; Ossipova et al., 2009) gave good rescue of infection. This stood in contrast to the substitution of cysteine 995 by serine (C995S), which did not rescue infection. The C995S mutant lacks ubiquitination activity due to a disrupted structure of the third RING domain (Berndt et al., 2011; Itoh et al., 2003). Staining of incoming vDNA confirmed that the truncation mutant 222-1006 and the C995S mutant failed to induce the genome release from the particles, unlike full length Mib1 (Supplemental Fig. 4).

Mib1 localizes to microtubules in centriolar satellites near the microtubule organizing center (MTOC). AdV traffics on microtubules to the vicinity of the nuclear envelope where it detaches from microtubules and binds to NPCs (Strunze et al., 2005; Wang et al., 2017). To distinguish if Mib1 acted on the capsid in transit from the MTOC to the NPC, or directly at the NPC-docked capsid, we infected HeLa-sgMib1 cells containing a tetracycline-inducible GFP-tagged Mib1. Upon virus internalization and arrest at the NPC, we added

doxycycline to induce the expression of GFP-Mib1, and analyzed the infected cells for vDNA uncoating. GFP-Mib1 expression was detectable as early as 1 h post induction, and led to the release of the vDNA from nearly all the capsids within 3 h of doxycycline treatment (Fig. 4D). By contrast, in cells that did not express GFP-Mib1, the vDNA remained confined inside the capsids.

This result suggests that Mib1 performs a ubiquitination reaction directly at the site where the capsids are docked at NPCs. This notion was supported by live cell imaging of atto565-labeled AdV-C5 particles in GFP-Mib1 expressing HeLa-sgMib1 cells, demonstrating that as early as 60 min post doxycycline addition, Mib1 puncta overlapped with viral capsids in the nuclear vicinity (Supplemental Movie 1). The interactions of GFP-Mib1 with the NPC-docked virions were transient, suggesting that Mib1 acts as a licensing factor on a cellular and/or a virion protein leading to vDNA uncoating. Remarkably, the expression pattern and dynamics of Mib1-GFP in uninfected cells showed rapid, linear and long-ranged trafficking of GFP-puncta, indistinguishable from infected cells (Supplemental Movie 2). We speculate that the Mib1 ubiquitination activity primes a cellular and/or virion protein for dissociation from the virion, and thereby unleashes the capsid disassembly reaction. Alternatively, the ubiquitylation of a cellular inhibitor of the AdV uncoating reaction at the NPC could initiate the release of a break in virion uncoating. Regardless, the absence of Mib1 caused a very strong and highly specific entry phenotype at the NPC, comparable perhaps to temperature-sensitive virus mutants, such as the endosomal escape-defective AdV-C2-TS1 (Imelli et al., 2009), or the HSV-1 mutants defective in uncoating at the NPC (Huffman et al., 2017; Knipe et al., 1981). These AdV and HSV-1 mutants have pleiotropic defects in the virion due to lack of proteolytic maturation (Imelli et al., 2009; Jovasevic et al., 2008).

Mib1 is abundantly available in most organs (Schmidt et al., 2018), and also in professional antigen-presenting cells, such as macrophages, which are infected by AdV (Li et al., 2011; Stichling et al., 2018). Besides being involved in Notch/Delta signalling (Itoh et al., 2003), Mib1 is implicated in centriole biogenesis (Cajanek et al., 2015), cell migration (Mizoguchi et al., 2017) and ciliogenesis (Wang et al., 2016), underscoring an important role in development (Koo et al., 2005). Point mutations in Mib1 can manifest in an autosomal-dominant fashion and cause disease, such as left ventricular noncompaction, the third most common cardiomyopathy (Luxan et al., 2013). In differentiated somatic cells,

however, Mib1 offers a novel anti-viral host target, for example in the lung, liver, gastro-intestinal tract, or eye. Since Mib1 is highly conserved, with homology >95% in most mammals, and >91% in distant vertebrates such as Zebrafish (Apweiler et al., 2004), it may also support AdV infection in other species than *homo sapiens*. In sum, our study identifies an 'on demand' tunable mechanism for the delivery of vDNA into the nucleus and misdelivery to the cytoplasm (Fig. 4E). The ubiquitination activity of Mib1 licenses AdV uncoating at the NPC. Targeted perturbations of host functions can now be applied to explore the uncoating mechanism of the vDNA.

Contributions by authors

Conceptualization (MB, UFG); supervision, project administration and funding acquisition (UFG); formal analyses and validations, software, data curation, visualization, design and conduction of cell-based experiments (MB); electron microscopy experiments (MB, JWF, KB); genome-wide siRNA screen (BC, DS, ME); generation of viruses (MB, MS, SH); data analyses and interpretation (MB, MS, JWF, UFG); writing (MB, UFG); editing (MB, MS, JWF, UFG).

Declaration of interests

The authors declare no competing interests.

Acknowledgements

We thank Christian von Mering and Andrea Franceschini for help with early data analyses in the RNAi screen. We acknowledge Yohei Yamauchi for gifts of IAV, VSV-GFP, anti-NP antibodies and discussions, Stacey Efstathiou for HSV-1-GFP, Anja Ehrhardt for HAdV-A31, and Jana Döhner and Gery Barmettler for help with microscopy, as well as Karsten Weis, Christian Münz, Christoph Dehio, Pauli Rämö and members of the Greber lab for helpful discussions. This work received financial support from the Swiss National Science

Foundation (31003A_179256/1), SystemsX RTD InfectX (51RT 0_126008) and SystemsX MRD VirX (2014/264) to UFG, and the Human Frontiers in Science Program (HFSP, grant LT000348/2014) to JWF.

References

Adey, A., Burton, J.N., Kitzman, J.O., Hiatt, J.B., Lewis, A.P., Martin, B.K., Qiu, R., Lee, C., and Shendure, J. (2013). The haplotype-resolved genome and epigenome of the aneuploid HeLa cancer cell line. Nature *500*, 207-211.

Apweiler, R., Bairoch, A., Wu, C.H., Barker, W.C., Boeckmann, B., Ferro, S., Gasteiger, E., Huang, H., Lopez, R., Magrane, M.*, et al.* (2004). UniProt: the Universal Protein knowledgebase. Nucleic Acids Res *32*, D115-119.

Balistreri, G., Horvath, P., Schweingruber, C., Zund, D., McInerney, G., Merits, A., Muhlemann, O., Azzalin, C., and Helenius, A. (2014). The host nonsense-mediated mRNA decay pathway restricts Mammalian RNA virus replication. Cell Host Microbe *16*, 403-411.

Banerjee, I., Miyake, Y., Nobs, S.P., Schneider, C., Horvath, P., Kopf, M., Matthias, P., Helenius, A., and Yamauchi, Y. (2014). Influenza A virus uses the aggresome processing machinery for host cell entry. Science *346*, 473-477.

Bauch, A., Adamczyk, I., Buczek, P., Elmer, F.J., Enimanev, K., Glyzewski, P., Kohler, M., Pylak, T., Quandt, A., Ramakrishnan, C.*, et al.* (2011). openBIS: a flexible framework for managing and analyzing complex data in biology research. BMC Bioinformatics *12*, 468.

Berk, A.J. (2005). Recent lessons in gene expression, cell cycle control, and cell biology from adenovirus. Oncogene *24*, 7673-7685.

Berndt, J.D., Aoyagi, A., Yang, P., Anastas, J.N., Tang, L., and Moon, R.T. (2011). Mindbomb 1, an E3 ubiquitin ligase, forms a complex with RYK to activate Wnt/beta-catenin signaling. J Cell Biol *194*, 737-750.

Brinkman, E.K., Chen, T., Amendola, M., and van Steensel, B. (2014). Easy quantitative assessment of genome editing by sequence trace decomposition. Nucleic Acids Res *42*, e168.

Burckhardt, C.J., Suomalainen, M., Schoenenberger, P., Boucke, K., Hemmi, S., and Greber, U.F. (2011). Drifting motions of the adenovirus receptor CAR and immobile integrins initiate virus uncoating and membrane lytic protein exposure. Cell Host Microbe *10*, 105-117.

Cajanek, L., Glatter, T., and Nigg, E.A. (2015). The E3 ubiquitin ligase Mib1 regulates Plk4 and centriole biogenesis. J Cell Sci *128*, 1674-1682.

Carpenter, A.E., Jones, T.R., Lamprecht, M.R., Clarke, C., Kang, I.H., Friman, O., Guertin, D.A., Chang, J.H., Lindquist, R.A., Moffat, J.*, et al.* (2006). CellProfiler: image analysis software for identifying and quantifying cell phenotypes. Genome Biol *7*, R100.

Cassany, A., Ragues, J., Guan, T., Begu, D., Wodrich, H., Kann, M., Nemerow, G.R., and Gerace, L. (2015). Nuclear import of adenovirus DNA involves direct interaction of hexon with an N-terminal domain of the nucleoporin Nup214. J Virol *89*, 1719-1730.

Cook, J., and Radke, J. (2017). Mechanisms of pathogenesis of emerging adenoviruses. F1000Res *6*, 90.

Crameri, M., Bauer, M., Caduff, N., Walker, R., Steiner, F., Franzoso, F.D., Gujer, C., Boucke, K., Kucera, T., Zbinden, A.*, et al.* (2018). MxB is an interferon-induced restriction factor of human herpesviruses. Nat Commun *9*, 1980.

Daga, N., Eicher, S., Kannan, A., Casanova, A., Low, S.H., Kreibich, S., Andritschke, D., Emmenlauer, M., Jenkins, J.L., Hardt, W.D.*, et al.* (2018). Growth-restricting effects of siRNA transfections: a largely deterministic combination of off-target binding and hybridization-independent competition. Nucleic Acids Res.

Davison, A.J., Benko, M., and Harrach, B. (2003). Genetic content and evolution of adenoviruses. J Gen Virol *84*, 2895-2908.

Dejarnac, O., Hafirassou, M.L., Chazal, M., Versapuech, M., Gaillard, J., Perera-Lecoin, M., Umana-Diaz, C., Bonnet-Madin, L., Carnec, X., Tinevez, J.Y.*, et al.* (2018). TIM-1 Ubiquitination Mediates Dengue Virus Entry. Cell reports *23*, 1779-1793.

Deshaies, R.J., and Joazeiro, C.A. (2009). RING domain E3 ubiquitin ligases. Annu Rev Biochem *78*, 399-434.

Dhason, M.S., Wang, J.C., Hagan, M.F., and Zlotnick, A. (2012). Differential assembly of Hepatitis B Virus core protein on single- and double-stranded nucleic acid suggest the dsDNA-filled core is spring-loaded. Virology *430*, 20-29.

Flatt, J.W., and Greber, U.F. (2017). Viral mechanisms for docking and delivering at nuclear pore complexes. Semin Cell Dev Biol *68*, 59-71.

Franceschini, A., Meier, R., Casanova, A., Kreibich, S., Daga, N., Andritschke, D., Dilling, S., Ramo, P., Emmenlauer, M., Kaufmann, A.*, et al.* (2014). Specific inhibition of diverse pathogens in human cells by synthetic microRNA-like oligonucleotides inferred from RNAi screens. Proc Natl Acad Sci U S A *111*, 4548-4553.

Glauser, D.L., Seyffert, M., Strasser, R., Franchini, M., Laimbacher, A.S., Dresch, C., de Oliveira, A.P., Vogel, R., Buning, H., Salvetti, A.*, et al.* (2010). Inhibition of herpes simplex virus type 1 replication by adeno-associated virus rep proteins depends on their combined DNA-binding and ATPase/helicase activities. J Virol *84*, 3808-3824.

Goff, S.P. (2008). Knockdown screens to knockout HIV-1. Cell *135*, 417-420.

Greber, U.F. (2016). Virus and Host Mechanics Support Membrane Penetration and Cell Entry. J Virol *90*, 3802-3805.

Greber, U.F., and Flatt, J.W. (2019). Adenovirus Entry: From Infection to Immunity. Annu Rev Virol.

Greber, U.F., Nakano, M.Y., and Suomalainen, M. (1998). Adenovirus entry into cells: A quantitative fluorescence microscopy approach. In Adenovirus methods and protocols, in Meth Mol Med Vol 21, W.S.M. Wold, ed. (Totowa, NJ USA: Humana Press, Inc), pp. 217-230.

Greber, U.F., Webster, P., Weber, J., and Helenius, A. (1996). The role of the adenovirus protease on virus entry into cells. EMBO J *15*, 1766-1777.

Greber, U.F., Willetts, M., Webster, P., and Helenius, A. (1993). Stepwise dismantling of adenovirus 2 during entry into cells. Cell *75*, 477-486.

Green, V.A., and Pelkmans, L. (2016). A Systems Survey of Progressive Host-Cell Reorganization during Rotavirus Infection. Cell Host Microbe *20*, 107-120.

Greene, W., Zhang, W., He, M., Witt, C., Ye, F., and Gao, S.J. (2012). The ubiquitin/proteasome system mediates entry and endosomal trafficking of Kaposi's sarcoma-associated herpesvirus in endothelial cells. PLoS Pathog *8*, e1002703.

Gschweitl, M., Ulbricht, A., Barnes, C.A., Enchev, R.I., Stoffel-Studer, I., Meyer-Schaller, N., Huotari, J., Yamauchi, Y., Greber, U.F., Helenius, A.*, et al.* (2016). A SPOPL/Cullin-3 ubiquitin ligase complex regulates endocytic trafficking by targeting EPS15 at endosomes. eLife *5*.

Hao, L., He, Q., Wang, Z., Craven, M., Newton, M.A., and Ahlquist, P. (2013). Limited agreement of independent RNAi screens for virus-required host genes owes more to false-negative than false-positive factors. PLoS Comput Biol *9*, e1003235.

Hayer, A., Stoeber, M., Ritz, D., Engel, S., Meyer, H.H., and Helenius, A. (2010). Caveolin-1 is ubiquitinated and targeted to intralumenal vesicles in endolysosomes for degradation. J Cell Biol *191*, 615-629.

Hearing, P., and Shenk, T. (1983). The adenovirus type 5 E1A transcriptional control region contains a duplicated enhancer element. Cell *33*, 695-703.

Huffman, J.B., Daniel, G.R., Falck-Pedersen, E., Huet, A., Smith, G.A., Conway, J.F., and Homa, F.L. (2017). The C Terminus of the Herpes Simplex Virus UL25 Protein Is Required for Release of Viral Genomes from Capsids Bound to Nuclear Pores. J Virol *91*.

Imelli, N., Ruzsics, Z., Puntener, D., Gastaldelli, M., and Greber, U.F. (2009). Genetic reconstitution of the human adenovirus type 2 temperature-sensitive 1 mutant defective in endosomal escape. Virol J *6*, 174.

Itoh, M., Kim, C.H., Palardy, G., Oda, T., Jiang, Y.J., Maust, D., Yeo, S.Y., Lorick, K., Wright, G.J., Ariza-McNaughton, L.*, et al.* (2003). Mind bomb is a ubiquitin ligase that is essential for efficient activation of Notch signaling by Delta. Dev Cell *4*, 67-82.

Jovasevic, V., Liang, L., and Roizman, B. (2008). Proteolytic cleavage of VP1-2 is required for release of herpes simplex virus 1 DNA into the nucleus. J Virol *82*, 3311-3319.

Karlas, A., Machuy, N., Shin, Y., Pleissner, K.P., Artarini, A., Heuer, D., Becker, D., Khalil, H., Ogilvie, L.A., Hess, S.*, et al.* (2010). Genome-wide RNAi screen identifies human host factors crucial for influenza virus replication. Nature *463*, 818-822.

Kim, S.J., Fernandez-Martinez, J., Nudelman, I., Shi, Y., Zhang, W., Raveh, B., Herricks, T., Slaughter, B.D., Hogan, J.A., Upla, P.*, et al.* (2018). Integrative structure and functional anatomy of a nuclear pore complex. Nature *555*, 475-482.

Knipe, D.M., Batterson, W., Nosal, C., Roizman, B., and Buchan, A. (1981). Molecular genetics of herpes simplex virus. VI. Characterization of a temperature-sensitive mutant defective in the expression of all early viral gene products. J Virol *38*, 539-547.

Kobiler, O., Drayman, N., Butin-Israeli, V., and Oppenheim, A. (2012). Virus strategies for passing the nuclear envelope barrier. Nucleus *3*, 526-539.

Komander, D., and Rape, M. (2012). The ubiquitin code. Annu Rev Biochem *81*, 203-229.

Koo, B.K., Lim, H.S., Song, R., Yoon, M.J., Yoon, K.J., Moon, J.S., Kim, Y.W., Kwon, M.C., Yoo, K.W., Kong, M.P.*, et al.* (2005). Mind bomb 1 is essential for generating functional Notch ligands to activate Notch. Development *132*, 3459-3470.

Krishnan, M.N., Ng, A., Sukumaran, B., Gilfoy, F.D., Uchil, P.D., Sultana, H., Brass, A.L., Adametz, R., Tsui, M., Qian, F.*, et al.* (2008). RNA interference screen for human genes associated with West Nile virus infection. Nature *455*, 242-245.

Lam, E., Stein, S., and Falck-Pedersen, E. (2014). Adenovirus Detection by the cGAS/STING/TBK1 DNA Sensing Cascade. J Virol *88*, 974-981.

Lau, L., Gray, E.E., Brunette, R.L., and Stetson, D.B. (2015). DNA tumor virus oncogenes antagonize the cGAS-STING DNA-sensing pathway. Science *350*, 568-571.

Li, Q., Brass, A.L., Ng, A., Hu, Z., Xavier, R.J., Liang, T.J., and Elledge, S.J. (2009). A genome-wide genetic screen for host factors required for hepatitis C virus propagation. Proc Natl Acad Sci U S A *106*, 16410-16415.

Li, S., Wang, L., Berman, M., Kong, Y.Y., and Dorf, M.E. (2011). Mapping a dynamic innate immunity protein interaction network regulating type I interferon production. Immunity *35*, 426-440.

Lipovsky, A., Popa, A., Pimienta, G., Wyler, M., Bhan, A., Kuruvilla, L., Guie, M.A., Poffenberger, A.C., Nelson, C.D., Atwood, W.J.*, et al.* (2013). Genome-wide siRNA screen

identifies the retromer as a cellular entry factor for human papillomavirus. Proc Natl Acad Sci U S A *110*, 7452-7457.

Luisoni, S., Suomalainen, M., Boucke, K., Tanner, L.B., Wenk, M.R., Guan, X.L., Grzybek, M., Coskun, U., and Greber, U.F. (2015). Co-option of Membrane Wounding Enables Virus Penetration into Cells. Cell Host Microbe *18*, 75-85.

Luo, H. (2016). Interplay between the virus and the ubiquitin-proteasome system: molecular mechanism of viral pathogenesis. Current opinion in virology *17*, 1-10.

Luxan, G., Casanova, J.C., Martinez-Poveda, B., Prados, B., D'Amato, G., MacGrogan, D., Gonzalez-Rajal, A., Dobarro, D., Torroja, C., Martinez, F.*, et al.* (2013). Mutations in the NOTCH pathway regulator MIB1 cause left ventricular noncompaction cardiomyopathy. Nat Med *19*, 193-201.

Mano, M., Ippodrino, R., Zentilin, L., Zacchigna, S., and Giacca, M. (2015). Genome-wide RNAi screening identifies host restriction factors critical for in vivo AAV transduction. Proc Natl Acad Sci U S A *112*, 11276-11281.

Mantovani, F., and Banks, L. (2001). The human papillomavirus E6 protein and its contribution to malignant progression. Oncogene *20*, 7874-7887.

Marsh, M., and Helenius, A. (2006). Virus entry: open sesame. Cell *124*, 729-740.

Meier, R., Franceschini, A., Horvath, P., Tetard, M., Mancini, R., von Mering, C., Helenius, A., and Lozach, P.Y. (2014). Genome-wide small interfering RNA screens reveal VAMP3 as a novel host factor required for Uukuniemi virus late penetration. J Virol *88*, 8565-8578.

Mercer, J., Snijder, B., Sacher, R., Burkard, C., Bleck, C.K., Stahlberg, H., Pelkmans, L., and Helenius, A. (2012). RNAi screening reveals proteasome- and Cullin3-dependent stages in vaccinia virus infection. Cell reports *2*, 1036-1047.

Mertz, J., Tan, H., Pagala, V., Bai, B., Chen, P.C., Li, Y., Cho, J.H., Shaw, T., Wang, X., and Peng, J. (2015). Sequential Elution Interactome Analysis of the Mind Bomb 1 Ubiquitin Ligase Reveals a Novel Role in Dendritic Spine Outgrowth. Mol Cell Proteomics *14*, 1898-1910.

Minskaia, E., Nicholson, J., and Ryan, M.D. (2013). Optimisation of the foot-and-mouth disease virus 2A co-expression system for biomedical applications. BMC biotechnology *13*, 67.

Mizoguchi, T., Ikeda, S., Watanabe, S., Sugawara, M., and Itoh, M. (2017). Mib1 contributes to persistent directional cell migration by regulating the Ctnnd1-Rac1 pathway. Proc Natl Acad Sci U S A *114*, E9280-E9289.

Moyer, C.L., Wiethoff, C.M., Maier, O., Smith, J.G., and Nemerow, G.R. (2011). Functional genetic and biophysical analyses of membrane disruption by human adenovirus. J Virol *85*, 2631-2641.

Munger, K., Basile, J.R., Duensing, S., Eichten, A., Gonzalez, S.L., Grace, M., and Zacny, V.L. (2001). Biological activities and molecular targets of the human papillomavirus E7 oncoprotein. Oncogene *20*, 7888-7898.

Orazio, N.I., Naeger, C.M., Karlseder, J., and Weitzman, M.D. (2011). The adenovirus E1b55K/E4orf6 complex induces degradation of the Bloom helicase during infection. J Virol *85*, 1887-1892.

Ossipova, O., Ezan, J., and Sokol, S.Y. (2009). PAR-1 phosphorylates Mind bomb to promote vertebrate neurogenesis. Dev Cell *17*, 222-233.

Ostapchuk, P., Suomalainen, M., Zheng, Y., Boucke, K., Greber, U.F., and Hearing, P. (2017). The adenovirus major core protein VII is dispensable for virion assembly but is essential for lytic infection. PLoS Pathog *13*, e1006455.

Pacesa, M., Hendrickx, R., Bieri, M., Flatt, J.W., Greber, U.F., and Hemmi, S. (2017). Small-size recombinant adenoviral hexon protein fragments for the production of virus-type specific antibodies. Virol J *14*, 158.

Puntener, D., Engelke, M.F., Ruzsics, Z., Strunze, S., Wilhelm, C., and Greber, U.F. (2011). Stepwise loss of fluorescent core protein V from human adenovirus during entry into cells. J Virol *85*, 481-496.

Querido, E., Blanchette, P., Yan, Q., Kamura, T., Morrison, M., Boivin, D., Kaelin, W.G., Conaway, R.C., Conaway, J.W., and Branton, P.E. (2001). Degradation of p53 by

adenovirus E4orf6 and E1B55K proteins occurs via a novel mechanism involving a Cullin-containing complex. Genes Dev *15*, 3104-3117.

Ramo, P., Drewek, A., Arrieumerlou, C., Beerenwinkel, N., Ben-Tekaya, H., Cardel, B., Casanova, A., Conde-Alvarez, R., Cossart, P., Csucs, G.*, et al.* (2014). Simultaneous analysis of large-scale RNAi screens for pathogen entry. BMC Genomics *15*, 1162.

Robinson, M., Li, B., Ge, Y., Ko, D., Yendluri, S., Harding, T., VanRoey, M., Spindler, K.R., and Jooss, K. (2009). Novel immunocompetent murine tumor model for evaluation of conditionally replication-competent (oncolytic) murine adenoviral vectors. J Virol *83*, 3450-3462.

Roulin, P.S., Murer, L., and Greber, U.F. (2018). A single point mutation in the rhinovirus 2B protein reduces the requirement for phosphatidylinositol 4-kinase class 3beta in viral replication. J Virol.

Sanjana, N.E., Shalem, O., and Zhang, F. (2014). Improved vectors and genome-wide libraries for CRISPR screening. Nat Methods *11*, 783-784.

Schindelin, J., Arganda-Carreras, I., Frise, E., Kaynig, V., Longair, M., Pietzsch, T., Preibisch, S., Rueden, C., Saalfeld, S., Schmid, B.*, et al.* (2012). Fiji: an open-source platform for biological-image analysis. Nature Meth *9*, 676-682.

Schmidt, H.B., and Gorlich, D. (2016). Transport Selectivity of Nuclear Pores, Phase Separation, and Membraneless Organelles. Trends Biochem Sci *41*, 46-61.

Schmidt, T., Samaras, P., Frejno, M., Gessulat, S., Barnert, M., Kienegger, H., Krcmar, H., Schlegl, J., Ehrlich, H.C., Aiche, S.*, et al.* (2018). ProteomicsDB. Nucleic Acids Res *46*, D1271-D1281.

Schreiner, S., Wimmer, P., Sirma, H., Everett, R.D., Blanchette, P., Groitl, P., and Dobner, T. (2010). Proteasome-dependent degradation of Daxx by the viral E1B-55K protein in human adenovirus-infected cells. J Virol *84*, 7029-7038.

Shahin, V., Hafezi, W., Oberleithner, H., Ludwig, Y., Windoffer, B., Schillers, H., and Kuhn, J.E. (2006). The genome of HSV-1 translocates through the nuclear pore as a condensed rod-like structure. J Cell Sci *119*, 23-30.

Shen, M.W., Arbab, M., Hsu, J.Y., Worstell, D., Culbertson, S.J., Krabbe, O., Cassa, C.A., Liu, D.R., Gifford, D.K., and Sherwood, R.I. (2018). Predictable and precise template-free CRISPR editing of pathogenic variants. Nature *563*, 646-651.

Slaymaker, I.M., Gao, L., Zetsche, B., Scott, D.A., Yan, W.X., and Zhang, F. (2016). Rationally engineered Cas9 nucleases with improved specificity. Science *351*, 84-88.

Smith, J.A., White, E.A., Sowa, M.E., Powell, M.L., Ottinger, M., Harper, J.W., and Howley, P.M. (2010). Genome-wide siRNA screen identifies SMCX, EP400, and Brd4 as E2-dependent regulators of human papillomavirus oncogene expression. Proc Natl Acad Sci U S A *107*, 3752-3757.

Stichling, N., Suomalainen, M., Flatt, J.W., Schmid, M., Pacesa, M., Hemmi, S., Jungraithmayr, W., Maler, M.D., Freudenberg, M.A., Pluckthun, A.*, et al.* (2018). Lung macrophage scavenger receptor SR-A6 (MARCO) is an adenovirus type-specific virus entry receptor. PLoS Pathog *14*, e1006914.

Strunze, S., Engelke, M.F., Wang, I.H., Puntener, D., Boucke, K., Schleich, S., Way, M., Schoenenberger, P., Burckhardt, C.J., and Greber, U.F. (2011). Kinesin-1-mediated capsid disassembly and disruption of the nuclear pore complex promote virus infection. Cell Host Microbe *10*, 210-223.

Strunze, S., Trotman, L.C., Boucke, K., and Greber, U.F. (2005). Nuclear targeting of adenovirus type 2 requires CRM1-mediated nuclear export. Mol Biol Cell *16*, 2999-3009.

Su, W.C., Chen, Y.C., Tseng, C.H., Hsu, P.W., Tung, K.F., Jeng, K.S., and Lai, M.M. (2013). Pooled RNAi screen identifies ubiquitin ligase Itch as crucial for influenza A virus release from the endosome during virus entry. Proc Natl Acad Sci U S A *110*, 17516-17521.

Suomalainen, M., Luisoni, S., Boucke, K., Bianchi, S., Engel, D.A., and Greber, U.F. (2013). A direct and versatile assay measuring membrane penetration of adenovirus in single cells. J Virol *87*, 12367-12379.

Szklarczyk, D., Morris, J.H., Cook, H., Kuhn, M., Wyder, S., Simonovic, M., Santos, A., Doncheva, N.T., Roth, A., Bork, P.*, et al.* (2017). The STRING database in 2017: quality-

controlled protein-protein association networks, made broadly accessible. Nucleic Acids Res *45*, D362-D368.

Trotman, L.C., Mosberger, N., Fornerod, M., Stidwill, R.P., and Greber, U.F. (2001). Import of adenovirus DNA involves the nuclear pore complex receptor CAN/Nup214 and histone H1. Nat Cell Biol *3*, 1092-1100.

Varghese, R., Mikyas, Y., Stewart, P.L., and Ralston, R. (2004). Postentry neutralization of adenovirus type 5 by an antihexon antibody. J Virol *78*, 12320-12332.

Vijayalingam, S., and Chinnadurai, G. (2013). Adenovirus L-E1A activates transcription through mediator complex-dependent recruitment of the super elongation complex. J Virol *87*, 3425-3434.

Villumsen, B.H., Danielsen, J.R., Povlsen, L., Sylvestersen, K.B., Merdes, A., Beli, P., Yang, Y.G., Choudhary, C., Nielsen, M.L., Mailand, N.*, et al.* (2013). A new cellular stress response that triggers centriolar satellite reorganization and ciliogenesis. EMBO J *32*, 3029-3040.

Walther, T.C., Fornerod, M., Pickersgill, H., Goldberg, M., Allen, T.D., and Mattaj, I.W. (2001). The nucleoporin Nup153 is required for nuclear pore basket formation, nuclear pore complex anchoring and import of a subset of nuclear proteins. EMBO J *20*, 5703-5714.

Wang, I.H., Burckhardt, C.J., Yakimovich, A., and Greber, U.F. (2018). Imaging, Tracking and Computational Analyses of Virus Entry and Egress with the Cytoskeleton. Viruses *10*, 10.3390/v10040166.

Wang, I.H., Burckhardt, C.J., Yakimovich, A., Morf, M.K., and Greber, U.F. (2017). The nuclear export factor CRM1 controls juxta-nuclear microtubule-dependent virus transport. J Cell Sci *130*, 2185-2195.

Wang, I.H., Suomalainen, M., Andriasyan, V., Kilcher, S., Mercer, J., Neef, A., Luedtke, N.W., and Greber, U.F. (2013). Tracking viral genomes in host cells at single-molecule resolution. Cell Host Microbe *14*, 468-480.

Wang, L., Lee, K., Malonis, R., Sanchez, I., and Dynlacht, B.D. (2016). Tethering of an E3 ligase by PCM1 regulates the abundance of centrosomal KIAA0586/Talpid3 and promotes ciliogenesis. eLife *5*.

Watanabe, T., Watanabe, S., and Kawaoka, Y. (2010). Cellular networks involved in the influenza virus life cycle. Cell Host Microbe *7*, 427-439.

Wiethoff, C.M., Wodrich, H., Gerace, L., and Nemerow, G.R. (2005). Adenovirus protein VI mediates membrane disruption following capsid disassembly. J Virol *79*, 1992-2000.

Witte, R., Andriasyan, V., Georgi, F., Yakimovich, A., and Greber, U.F. (2018). Concepts in Light Microscopy of Viruses. Viruses *10*, 10.3390/v10040202.

Wolfrum, N., and Greber, U.F. (2013). Adenovirus signalling in entry. Cell Microbiol *15*, 53-62.

Wu, K.X., Phuektes, P., Kumar, P., Goh, G.Y., Moreau, D., Chow, V.T., Bard, F., and Chu, J.J. (2016). Human genome-wide RNAi screen reveals host factors required for enterovirus 71 replication. Nat Commun *7*, 13150.

Yakimovich, A., Gumpert, H., Burckhardt, C.J., Lutschg, V.A., Jurgeit, A., Sbalzarini, I.F., and Greber, U.F. (2012). Cell-free transmission of human adenovirus by passive mass transfer in cell culture simulated in a computer model. J Virol *86*, 10123–10137.

Yamauchi, Y., Boukari, H., Banerjee, I., Sbalzarini, I.F., Horvath, P., and Helenius, A. (2011). Histone deacetylase 8 is required for centrosome cohesion and influenza A virus entry. PLoS Pathog *7*, e1002316.

Yamauchi, Y., and Greber, U.F. (2016). Principles of Virus Uncoating: Cues and the Snooker Ball. Traffic *17*, 569-592.

Figures and Legends

Fig. 1: Mib1 is an essential host factor for AdV infection.

(A) Overview of the experimental workflow of the genome-wide siRNA screen in HeLa cells.

(B) The infection Z-scores from the genome-wide screen are plotted per gene in ascending order. The Z-score of Mib1 is indicated. See also Supplemental Tables 1, 2, 3.

(C) A549 cells transfected with siRNAs against GFP, Mib1 or a non-targeting control were infected with AdV-C5-GFP at MOI 0.3 for 24 h. Nuclei were stained with DAPI, cells analyzed by fluorescence microscopy, and infection scored by measuring the GFP signal over the nuclei. The mean ± s.d. is shown (n = 3 replicates). Statistical significance was assessed using one-way ANOVA with Holm-Sidak correction for multiple comparisons.

(D) A549 cells transfected with siRNAs were lysed at 48 h post transfection. Proteins were separated by SDS-PAGE and probed for Mib1 or GAPDH by Western blotting.

(E) A549, HeLa, or WI-38 cells were transfected with siRNAs and infected with AdV-C5-GFP as in (C). n = 3 biologically independent experiments. The *P* value was determined using an unpaired t-test.

(F) Monoclonal HeLa-sgMib1 cells or control HeLa-sgNT cells were infected with different wild-type AdVs for 24 h. After fixation, cells were stained with a pan-hexon antibody and DAPI. Infection was scored by percentage of hexon-positive nuclei. Representative images shown. Scale bar, 100 µm. n = 3 biologically independent experiments. The *P* values were assessed using unpaired t-tests.

(G) HeLa-sgNT or HeLa-sgMib1 cells were transduced with an empty lentivirus or lentivirus encoding Mib1. At 48 h post transduction, cells were infected with AdV-C5-wt, fixed at 24 h pi, and stained for the viral protein VI and DAPI. Infection was scored by percentage of protein VI-positive nuclei. Scale bar, 100 µm. n = 3 biologically independent experiments. Statistical significance was assessed using a one-way ANOVA with Holm-Sidak correction. ***, $p<0.0001$.

(H) HeLa-sgNT or HeLa-sgMib1 cells were transduced with an empty lentivirus or lentivirus encoding Mib1, lysed 48 h post transduction, and processed as in (D). All bar graphs show the mean ± s.d.

Fig. 2: Mib1 depletion does not affect the early steps of viral entry.

(A) AdV-C5 entry schematic.

(B) AdV-C5 was bound to siRNA-treated HeLa cells for 1 h on ice. The virus inoculum was removed and cells were fixed, followed by immunostaining of hexon, DAPI staining, AlexaFluor 647-conjugated succinimidyl ester (cell contents) and imaging by confocal microscopy. Data from one representative experiment is shown. n = 3 independent experiments gave similar results. *P* value was determined using a Mann-Whitney test.

(C) AlexaFluor 488-labeled AdV-C5 was bound to siRNA-treated HeLa cells for 1 h on ice. Unbound virus was washed away, and bound virus internalized for 0, 10, or 20 min at 37°C. Cells were treated with anti-hexon antibody for 1 h, fixed, permeabilized, and stained with secondary antibody, DAPI, and analyzed by confocal microscopy. Only virus particles on the cell surface are positive for anti-hexon. Representative data from one of n = 3 independent experiments is shown. *P* values were determined using a non-parametric ANOVA (Kruskal-Wallis test) with Dunn's correction for multiple comparisons.

(D) siRNA-treated HeLa cells were infected as in (C), fixed, and processed for immunostaining with anti-protein VI and DAPI. Representative data from one of n = 3 independent experiments. *P* values were assessed using a Kruskal-Wallis test with Dunn's correction.

(E) AdV-C5 was bound to A549-sgNT or A549-sgMib1 cells for 1 h on ice. Unbound virus was washed away, cells fixed immediately (or after an additional 1, 3, 5 or 8 h of incubation at 37°C), processed for immunostaining with anti-hexon, DAPI, and succinimidyl ester, and imaged by confocal microscopy. Virus nuclear targeting was scored as percentage of capsids over the DAPI mask. n = 3 experiments gave similar results. *P* values were calculated using a Kruskal-Wallis test with Dunn's correction. Mean ± s.d. is shown for each graph.

Fig. 3: Genome release is impaired in Mib1-KO cells.

(A) HeLa-sgNT and HeLa-sgMib1 cells were incubated with AdV-C5 at 37°C for 1 h. Unbound virus was washed away and cells returned to 37°C, fixed at 1, 2, or 5 h pi and processed for thin-slice transmission electron microscopy. Viral capsids near the nuclear envelope were counted and plotted. Data from one of n = 2 independent experiments is shown. *P* values were determined using a Kruskal-Wallis test with Dunn's correction.

(B) HeLa-sgNT and HeLa-sgMib1 cells were infected as in (A), fixed at 7 h pi, and processed for electron microscopy. Representative images of NPCs from slices of different cells are shown. Almost no viral particles were found in the sgNT cells. Two independent experiments yielded similar results. Scale bar, 100 nm. n, nucleus; c, cytoplasm.

(C) HeLa-sgNT or HeLa-sgMib1 cells were incubated with genome-labeled AdV-C5-EdC for 1 h on ice, washed, transferred to 37°C, and fixed at the indicated timepoints. Capsids were stained with anti-hexon, and viral genomes visualized by click chemistry with an N_3-AlexaFluor 488. Nuclei were stained with DAPI and cell outlines with AlexaFluor 647-conjugated succinimidyl ester, and cells analyzed by confocal microscopy. Incoming viral genomes were segmented and their corresponding hexon intensity plotted. Each dot represents one viral genome. Data collected in one of n = 3 independent experiments is shown. *P* values were assessed using a Kruskal-Wallis test with Dunn's correction. Error bars depict the mean ± s.d..

(D) Representative images from the dataset collected in (C). Arrows show free cytoplasmic genomes, arrowheads depict nuclear genomes. Scale bar, 10 µm. n = 3 independent experiments gave similar results. Images are maximum projections.

Fig. 4: Mib1 ubiquitination activity is required for AdV genome release.

(A) Schematic representation of Mib1 domains.

(B) HeLa-sgMib1 cells were transduced with lentivirus expressing the indicated constructs. Non-transduced HeLa-sgNT cells were included as a control. 48 h post transduction, cells

were infected with AdV-C5-GFP. At 24 h pi, cells were fixed, and nuclei stained with DAPI before imaging by fluorescence microscopy. Infection was scored by measuring GFP intensity over nuclei. Error bars depict the mean ± s.d. of three replicates in one representative of n = 3 independent experiments. Statistical significance was assessed by using a one-way ANOVA with Holm-Sidak correction for multiple comparisons. ***, $p<0.0001$.

(C) HeLa-sgMib1 cells were transduced as in (B) and subsequently lysed and processed for SDS-PAGE and Western blotting. Expression of flag-Mib1 mutants was probed with an anti-flag antibody, flag-Cas9 served as a loading control.

(D) HeLa-sgMib1 cells carrying a tetracycline-inducible GFP-Mib1 cassette were incubated for 1 h with AdV-C5-EdC. Unbound virus was washed away and internalized virus capsids were allowed to reach the nucleus for another 2 h. GFP-Mib1 expression was subsequently induced with 1 µg/ml doxycycline for 1 or 3 h, after which cells were fixed, stained for vDNA, hexon, and nuclei, and imaged via confocal fluorescence microscopy. Images are maximum projections. n = 3 independent experiments gave similar results. Scale bar, 10 µm. See also Supplemental Fig. 4.

(E) Schematic model depicting the block in AdV DNA uncoating at the nuclear pore complex (NPC) in the absence of Mib1. Induced expression of the E3 ubiquitin (Ub) ligase Mib1 licenses AdV uncoating, vDNA nuclear import and misdelivery, and leads to infection.

STAR Methods

LEAD CONTACT AND MATERIALS AVAILABILITY

Further information and requests for resources and reagents should be directed to and will be fulfilled by the Lead Contact, Professor Urs Greber (urs.greber@imls.uzh.ch). All reagents generated in this study are available from the Lead Contact with a completed Materials Transfer Agreement.

EXPERIMENTAL MODEL AND SUBJECT DETAILS

Virus construction and growth

All AdVs were grown in human A549 or HeLa-ATCC cells and purified over two cesium chloride gradients as previously described (Greber et al., 1996; Greber et al., 1993). AdV-C5 (wt300) has been previously described (Hearing and Shenk, 1983). AdV-C5-E1A-FS2A-GFP was constructed by inserting an enhanced GFP (GFP) cassette at the end of the E1A gene along with a furin cleavage site (FS) and a 'ribosome-skipping' F2A sequence derived from foot and mouth disease virus (Minskaia et al., 2013; Pacesa et al., 2017; Robinson et al., 2009), leading to expression of stand-alone GFP under the E1A promoter. This is akin to a mouse AdV-1 expressing murine granulocyte-macrophage colony-stimulating factor and human AdV-B3 expressing a GFP reporter (Pacesa et al., 2017; Robinson et al., 2009). AdV-C2-ΔE3B-CMV-GFP has been previously described and contains a GFP cassette under a CMV promoter in place of the non-essential E3B gene region (Yakimovich et al., 2012). Genome-labeled AdV-C5-EdC was produced by growing the virus in A549 cells in the presence of 2.5 μM EdC (5-Ethynyl-2′-deoxycytidine, Jena Biosciences) as described (Wang et al., 2013). Capsid-labeled AdV-C5-atto565 and AdV-C5-AlexaFluor 488 were generated as previously described (Burckhardt et al., 2011; Greber et al., 1998). A GFP-expressing VSV-G pseudotyped lentivirus (LV-GFP) was constructed by cloning a GFP cassette into the multiple cloning site of the lentiviral vector pLVX-IRES-puro (Clontech). The lentivirus was then rescued as described below. GFP-expressing vesicular stomatitis virus (VSV-GFP) was kindly provided by Y. Yamauchi

(University of Bristol) (Hayer et al., 2010). Influenza A virus strain X31 (H3N2) was purchased from Virapur. GFP-expressing HSV-1 strain C12 was kindly provided by S. Efstathiou (University of Cambridge)(Glauser et al., 2010).

Generation of lentiviral particles

$4.5x10^6$ HEK293T cells were seeded on a 10 cm dish. The next day, the cells were transfected with 3.4 µg pVSV-G (Clontech), 6.5 µg pCMV-dR8.91-Gag-Pol (kindly provided by J. Pavlovic, University of Zurich), and 10 µg of lentiviral expression plasmid using the calcium phosphate method. The culture supernatant was changed to fresh medium the following morning, and the supernatant containing the lentiviral particles was harvested at 2 days post transfection and filtered through a 0.45 µm filter before storage at -80°C. For experiments, cells were transduced with the lentiviral vectors at a MOI of 0.5 and selected with 2 µg/ml puromycin or 10 µg/ml blasticidin.

Reagents

Anti-AdV pan-hexon (mouse, MAB8052) and anti-E1A (mouse, 05-599) were purchased from Millipore. Anti-Mib1 (rabbit, ab124929) and anti-NPC Mab414 (mouse, ab24609) were purchased from abcam. Anti-GAPDH (mouse, MA5-15738), anti-flag (mouse, MA5-91878), and all secondary antibodies used for immunofluorescence were purchased from Thermo Fisher Scientific. Polyclonal anti-flag (rabbit, F7425) was purchased from Sigma-Aldrich. All HRP-conjugated secondary antibodies used for Western Blotting were purchased from Cell Signaling Technologies. Rabbit polyclonal anti-AdV protein VI has been previously characterized (Burckhardt et al., 2011). Mouse monoclonal anti-AdV hexon 9C12 antibody was produced from hybridoma cell lines(Varghese et al., 2004). Mouse monoclonal anti-IAV NP antibody (HB-65) was a kind gift from Y. Yamauchi (University of Bristol). Lipofectamine RNAiMAX (13778075), Alexa Fluor 647 NHS Ester (A37566), Alexa Fluor 488 Azide (A10266), and Alexa Fluor 594 Azide (A10270) were purchased from Thermo Fisher Scientific. THPTA (762342), aminoguanidine hydrochloride (396494), copper sulfate (61230), and (+)-sodium L-ascorbate (11140) were purchased from Sigma-Aldrich. Doxycycline (631311) was purchased from Clontech.

METHOD DETAILS

Cell cultures

HEK293T, HeLa, A549, and WI-38 cells were maintained in Dulbecco's Modified Eagle's Medium (Gibco). Medium was supplemented with non-essential amino acids (Thermo Fisher) and 10% fetal calf serum (Gibco). During infection experiments, the medium was additionally supplemented with 100 U/ml penicillin and 100 µg/ml streptomycin. The cells were grown at 37°C in a 5% CO_2 atmosphere for no longer than 20 passages.

Genome-wide siRNA screen

The RNA interference screen was performed as part of the InfectX consortium using a commercially available pooled genome-wide siRNA library from Dharmacon (Ramo et al., 2014). The screen was conducted in HeLa CCL-2 cells in a 384-well plate format in two biological replicates. In each experiment, 25 µl of RNAiMAX (Invitrogen)/DMEM (0.1 µl / 24.9 µl) mixture was added to each well of the screening plates containing 1.6 pmol siRNA diluted in 5 µl RNase-free ddH2O, after which the plates were incubated at room temperature (RT) for 1 h. Seven hundred HeLa cells were add per well in a volume of 50 µl DMEM/10% FCS, resulting in a final concentration of 6.7% FCS. Plates were incubated at 37°C and 5% CO_2 for 72 h prior to infection. All liquid handling stages of infection, fixation, and immunofluorescence (IF) staining were performed on the automated pipetting system Well Mate (Thermo Scientific Matrix) and washer Hydrospeed (Tecan). AdV-C2-ΔE3B-GFP was added to the cells at a MOI of 0.1 in 10 µl of infection media (DMEM supplemented with L-glutamine, 10% FCS, 1% Pen/Strep, Invitrogen). The cells were incubated at 37°C for 16 h and then fixed by adding 21 µl of 16% PFA directly to the culture supernatant for 45 min at RT or long-term storage at 4°C. Cells were washed 2 times with PBS containing 25 mM NH_4Cl and permeabilized with 25 µl 0.1% Triton X-100 (Sigma-Aldrich). After two washes with PBS the samples were incubated at RT for 1 h with 25 µl PBS containing DAPI (1 µg/ml, Sigma-Aldrich) and DY-647-phalloidin (0.4 U/ml, Dyomics), washed 3 times with PBS and stored until imaging in 50 µl PBS supplemented with NaN_3. Microscopy was performed with Molecular Devices ImageXpress microscopes. Nine sites per well in a 3x3 grid were imaged with a 10x S Fluor objective with 0.45 numerical aperature (NA) in a 12-bit dynamic range. Infection was scored by quantifying the GFP intensity over segmented nuclei (based on DAPI staining) and cell bodies (based

on actin staining) using CellProfiler. All data generated during the screen including raw and processed images were shared through the openBIS system (Bauch et al., 2011). For the identification of pro-viral candidates, genes known to be involved in transcription and translation (such as polymerases, transcription factors, ribosomal proteins) were excluded based on their gene ontology terms. siRNAs that led to a strong reduction of cell numbers in the screen were additionally excluded in the validation experiments.

String analysis

Gene Ontology (GO) enrichment analysis of the strongest 500 infection up- and downregulating hits was performed with the "cellular components enrichment" tool of the STRING database (http://string-db.org). Statistical significance for enrichment by genome-wide false discovery rate (FDR) was calculated using the STRING database (Szklarczyk et al., 2017).

Generation of CRISPR/Cas9 KO cell lines

For the generation of CRISPR/Cas9 knockout cells, we used a modified plasmid termed Lenti-eCas9. This plasmid was generated by replacing the Cas9 cassette from the lentiCRISPR v2 plasmid (Addgene #52961) (Sanjana et al., 2014) with the high-fidelity eCas9 from the eSpCas9(1.1) plasmid (Addgene #71814) (Slaymaker et al., 2016) by restriction cloning using XbaI and BamHI restriction sites. The sequences used as gRNA templates were 5'-GTTGGCGCTCGGGTAGTGCG-3' for Mib1 and 5'-(G)ACGGAGGCTAAGCGTCGCAA-3' for a non-targeting gRNA, where the (G) denotes a nucleotide added for robust transcription from the U6 promoter. The sequences were cloned into the BsmBI site according to the instructions of the Zhang lab (Sanjana et al., 2014). All plasmids were verified by Sanger sequencing. The plasmids were then used for the generation of lentiviral particles. HeLa and A549 cells were transduced with lentiviral supernatant. After two days, the cells were selected with 2 µg/ml puromycin until all non-transduced cells were dead (ca. 5 days). Surviving cells from wells in which at least 50% of the cells had died were then expanded and frozen down. HeLa-sgMib1 cells were furthermore subcloned by limiting dilution. Unless otherwise stated, all experiments were performed with HeLa-sgMib1 cells grown from a single clone (cl. 1).

For sequencing analysis of the genome-edited cells, HeLa-ATCC and HeLa-sgMib1 cells were each grown in a 10 cm dish. When they reached 90% confluence, cells were lysed in lysis buffer (20 mM Tris pH 8.0, 20 mM NaCl, 4 mM EDTA, 1% SDS) and sheared through a 22G needle. Proteins were digested by incubation with 450 µg proteinase K for 2 h at 55°C under agitation. RNA was digested by incubation with 200 µg RNase A for 1 h at 37°C. DNA was then isolated through two repeated phenol-chloroform extractions with a phenol:chloroform:isoamyl alcohol solution at ratios of 25:24:1, pH 8, and precipitated by addition of 1/10 the volume of 3M potassium acetate pH 5.2 and 2 volumes of EtOH followed by incubation at -20°C overnight. After washing with 70% EtOH, DNA pellets were resuspended in TE buffer (pH 8) and used for PCR amplification of a 300 bp stretch surrounding the Cas9 cut site on the Mib1 ORF using GoTaq polymerase (Promega) with the following two primers carrying an XhoI or an EcoRI restriction site at their 5' ends: 5'-TTGCTCCTCGAGCTATGAGTAACTCCCGGAATAAC-3' and 5'-AAAGGAGAATTCTCTCCATGATAACACACTGTG-3'. The resulting PCR product was then gel-purified and ligated into a XhoI/EcoRI-digested pBluescript vector, which was then transformed into DH5α bacteria. The following day, more than 25 colonies were picked, their plasmid DNA isolated, and the PCR insert was sequenced by Sanger sequencing. Every colony from the sgMib1 sample showed the insertion of a single thymidine. To corroborate this result, we sent the PCR product for sequencing without prior transformation to analyze the amplified DNA from all Mib1 alleles. We analyzed the sequences using the TIDE web tool (https://tide.deskgen.com/), which allows quantitative assessment of genome editing by sequence trace decomposition (Brinkman et al., 2014). This analysis showed that 98.2% of reads from the HeLa-sgMib1 cells contained the insertion of a single T, confirming that all alleles carried the same frame-shift mutation. This is not surprising as the inDelphi tool (https://indelphi.giffordlab.mit.edu) which predicts the outcome of CRISPR/Cas9-mediated gene editing based on the gRNA target sequence context yields a high probability (>70% in human cancer cell lines) for a 1-bp insertion for this particular gRNA targeting site (Shen et al., 2018). A list of all used oligonucleotides is available in Supplemental Table 4.

Construction of expression plasmids

For constitutive expression, the lentiviral vector pLVX-IRES-puro (Clontech) was used. The Mib1 sequence was amplified by PCR from p3HA-hMib1 (Addgene #33317) with 5'-

TAAGCAGAATTCATGAGTAACTCCCGGAATAACC-3' and 5'-TGCTTAGCGGCCGCGGAATTCGCCCTTTCTTTAC-3' and cloned into the multiple cloning site (EcoRI/NotI) of pLVX-IRES-puro. To prevent cleavage of the re-introduced Mib1 gene by the Cas9/sgMib1 complex, the gRNA targeting site of Mib1 was mutated without changing the amino acid sequence via site-directed mutagenesis with the Q5 site-directed mutagenesis kit (New England Biolabs) according to the manufacturer's instructions with 5'-agttgtcagaGGCCCGGACTGGAAGTGG-3' and 5'-cttgcccctacCCCTTCCACCATCACCCG-3'. For detection of the Mib1 mutants, a flag-tag was introduced at the N-terminus of Mib1 using site-directed mutagenesis with 5'-cgattacaaggatgacgatgacaagggtggaggcggttccAGTAACTCCCGGAATAAC-3' and 5'-atgtcatgatctttataatcaccgtcatggtctttgtagtcCATGAATTCACCGGAAATAG-3'. The Mib1 point and truncation mutants were constructed by site-directed mutagenesis with the primers in Supplemental list of oligonucleotides.

For inducible expression, we first created a tetracycline-inducible lentiviral vector of the pLVX-IRES-puro backbone termed pLVX-tet-BSD which has been previously described (Roulin et al., 2018). pLVX-tet-BSD was constructed by replacing the CMV promoter, IRES, and puromycin resistance gene in pLVX-IRES-Puro with a tetracycline response element (TRE) followed by a multiple cloning site and an expression cassette containing a blasticidine deaminase (BSD), a P2A sequence, and a reverse Tet repressor (rTetR) under a constitutive EF-1α core promoter. GFP-Mib1 was constructed by insertion of Mib1 from p3HA-hMib1 into the XhoI and EcoRI sites of pGFP-C1 using 5'-TTGCTCCTCGAGCTATGAGTAACTCCCGGAATAAC-3' and 5'-TGGCAAGAATTCGGAATTCGCCCTTTCTTTAC-3' as PCR primers. The GFP-Mib1 sequence was then transferred from pGFP-Mib1 to pLVX-tet-BSD by restriction digest. pLVX-tet-BSD-GFP-Mib1 was then used to generate lentiviral particles for transduction of HeLa-sgMib1 cells. Transduced cells were selected with 10 µg/ml blasticidin for 7 days and then used for experiments or frozen down.

SDS-PAGE

Cells from a 24-well plate were washed with PBS, lysed in 200 µl SDS-PAGE lysis buffer (200 mM Tris pH 6.8, 10% glycerol, 5 mM EDTA, 0.02% bromphenol blue, 5% SDS, 50 mM DTT) and boiled for 5 min at 95°C. Lysates were then loaded onto a SDS-PAGE gel

and transferred to a PVDF membrane (Amersham). After blocking with blocking solution (5% milk powder in 20 mM Tris, 150 mM NaCl, 0.1% Tween-20, pH 7.5), the membrane was incubated with primary and secondary antibodies diluted in blocking solution at 4°C overnight or 1h at RT, with 4 washes of TBST in between. HRP-coupled secondary antibody was detected using the ECL reagent (GE Healthcare). Primary antibodies were used at the following dilutions: anti-GAPDH 1:2500, anti-flag 1:1000, anti-Mib1 1:1000, anti-AdV E1A M73 1:500. Secondary antibodies used in Western blotting were goat anti-rabbit-HRP (Cell Signaling, 7074) and goat anti-mouse-HRP (Cell Signaling, 7076) used at 1:5000 dilution.

siRNA transfections

Two pmol siRNAs were diluted in a mixture of 9.85 µl Optimem and 0.15 µl RNAiMAX and spotted in a black 96-well plate (Greiner Bio-One). After 15 min incubation, 3000 cells were added per well in a volume of 90 µl DMEM supplemented with 10% FCS and nonessential amino acids (NEAA). The cells were typically incubated for 48 h before further treatment. The final siRNA concentration for all experiments was 20 nM. Unless stated otherwise, siMib1 #2 (Dharmacon) was used for depletion of Mib1 due to its strong knockdown efficiency.

Infection

Cells in a black 96-well imaging plate were ca. 50% confluent at the time of infection. The virus was diluted in infection medium (DMEM supplemented with 2% FCS, non-essential amino acids, pen/strep) to reach an infection of 20-60%. The culture supernatant was aspirated and 100 µl of infection mix was added to the cells. For all AdV and lentiviral infections, the cells were fixed at 24 h pi with 4% PFA. For infections with HSV-1, VSV, and IAV, the cells were fixed at 7 h pi. After fixation, remaining PFA was quenched with 25 mM NH_4Cl diluted in PBS for 5-10 min, followed by permeabilization with 0.5% Triton X-100 in PBS for 3-5 min. If the virus carried a GFP transgene cassette, the cells were stained with DAPI at a concentration of 1 µg/ml in PBS for 3-5 min. For wild-type viruses, the cells were stained with the following primary antibodies diluted in blocking buffer (10% goat serum diluted in PBS) for 1 h at 4°C: mouse anti-hexon (Millipore, MAB8052) or rabbit anti-protein VI (Burckhardt et al., 2011) for AdV, and mouse anti-NP (ATCC, HB-65) for IAV. After three washes of 4 min each in PBS, the cells were stained with secondary

antibody (goat anti-rabbit-AlexaFluor 488 or goat anti-mouse-AlexaFluor 488, Thermo Fisher) diluted in blocking buffer containing 1 µg/ml DAPI for 30 min at RT. After three more washes of 4 min in PBS, the cells were imaged in a Molecular Devices high-throughput microscope (IXM-XL or IXMc) in widefield mode with a 20x objective. For quantification of infection with CellProfiler (Carpenter et al., 2006), the nuclei were segmented according to the DAPI signal and the GFP intensity over the nuclear mask was measured.

Endocytosis and protein VI exposure

Forty thousand HeLa cells were reverse-transfected with 20 nM siNT (Dharmacon, Cat# D-001810-01-05) or siMib1 (Dharmacon) onto a cover slip in a 24-well plate. At 2 days post transfection, the cells were incubated with atto565-labeled AdV-C5 (AdV-C5-atto565) diluted in cold binding medium (Hepes-buffered RPMI supplemented with 0.2% bovine serum albumin) for 1 h on ice. Unbound virus was washed away three times with PBS, fresh medium was added, and cells were moved to a 37°C water bath to allow internalization of viral particles for 0, 10, or 20 min. Cells were then inverted onto a 30 µl droplet of 9C12 anti-hexon antibody (Varghese et al., 2004) diluted in cold binding medium and placed on ice for 1 h. The cover slips were then transferred back into the wells, washed 3x with PBS, and fixed with 4% PFA for 15 min at RT. The samples were then quenched with 25 mM NH_4Cl for 5-10 min and permeabilized with 0.5% Triton X-100 in PBS for 3-5 min at RT. For immunostaining, the coverslips were inverted onto a 30 µl droplet of antibody diluted in blocking buffer (10% goat serum in PBS) containing an affinity-purified rabbit anti-protein VI antibody (Suomalainen et al., 2013) at 4°C for 1 h. After three washes of PBS for 4 min each, the cells were incubated with the appropriate secondary antibodies and the nuclei were stained with DAPI. The samples were imaged on a Leica SP8 confocal laser scanning microscope (cLSM) with a 63x objective and a zoom factor of two. Z-stacks were acquired with intervals of 0.5 µm across the entire height of the cells. Sequential acquisition was between frames with line averaging (depending on the signal-to-noise ratio) at a scanning speed of 700 Hz. After recording the images, virus capsids were segmented using CellProfiler based on the atto565 signal. The signal from the hexon antibody determined whether the particle was outside or inside the plasma membrane. The signal from the protein VI antibody indicated successful exposure of protein VI, as the antibody cannot penetrate the virus capsids.

Virus binding

Forty thousand HeLa cells were reverse-transfected with 20 nM siNT or siMib1 onto a cover slip in a 24-well plate. At 2 days post transfection, the cells were incubated with AdV-C5 diluted in cold binding medium on ice for 1 h. Subsequently, unbound virus was washed away with PBS and cells were fixed with 4% PFA. After fixation, remaining PFA was quenched and cells were permeabilized and stained with 9C12 anti-hexon antibody. Cell nuclei were stained with DAPI and cell outlines with AlexaFluor 647-conjugated succinimidyl ester. Cells were imaged on a Leica SP8 confocal microscope as described above. Nuclei were segmented based on the DAPI signal, cell outlines based on succinimidyl ester, and virus capsids based on the antibody signal.

Nuclear targeting

Eighty thousand A549-sgNT or A549-sgMib1cells were seeded on cover slips in a 24-well plate. The following day, cells were incubated with wt AdV-C5 in cold binding medium for 1 h on ice. Unbound virus was washed away, and cells were either fixed with 4% PFA, or given fresh medium and placed in the incubator for 1, 3, 5, or 8 additional hours. After fixation, remaining PFA was quenched and cells were permeabilized and stained with 9C12 anti-hexon antibody. Cell nuclei were stained with DAPI and cell outlines with succinimidyl ester. Cells were imaged on a Leica SP8 confocal microscope as described above. For determination of nuclear targeting efficiency of virus, nuclei were segmented based on the DAPI signal, cells based on the succinimidyl ester signal, and capsids based on the antibody signal in maximum projection images. The number of capsids over the nuclear mask was then set in relation to the number of capsids over the entire cell.

Click chemistry and vDNA analysis

Cells grown on cover slips were incubated with genome-labeled AdV-C5-EdC (Wang et al., 2013) for various time points. After fixation, quenching, and permeabilization, samples were stained for incoming capsids with the 9C12 anti-hexon antibody. After primary and secondary antibody incubation, the cover slips were inverted onto a 30 µl droplet of click reaction mix for 2 h at RT. The freshly prepared click reaction mix consisted of 10 µM AlexaFluor 594- or AlexaFluor 488-conjugated azide (Thermo Fisher Scientific), 1 mM $CuSO_4$, and 10 mM sodium ascorbate in the presence of 1 mM THPTA and 10 mM

aminoguanidine (AG) in PBS. Samples were stained with DAPI and imaged with a Leica SP8 cLSM as described above. Single viral genomes and/or capsids were segmented according to the corresponding signal using CellProfiler.

Expression of Mib1 and Mib1 mutants

HeLa-sgMib1 cells were transduced with lentivirus containing expression cassettes of Mib1 or Mib1 mutants under a CMV promoter. Two days after transduction, the cells were infected with AdV-C5-GFP for 24h and the infection efficiency was quantified as described above. For the analysis of incoming vDNA, cells were incubated with AdV-C5-EdC for 1 h on ice followed by 3 h at 37°C. Cells were then processed for immunostaining and click chemistry. For analysis of Mib1 expression, cells were lysed in SDS-PAGE lysis buffer, and proteins were separated via SDS-PAGE, followed by Western blotting with rabbit anti-flag antibody at 1:1000 dilution to detect the flag-Mib1 proteins.

Doxycycline-induced expression of Mib1

HeLa-sgMib1 cells which had been transduced with LVX-tet-BSD-GFP-Mib1 and selected for seven days with blasticidin were seeded on cover slips and infected with AdV-C5-EdC. After 1 h at 37°C, cells were washed and given fresh medium. The cells were placed back at 37°C for an additional 2 h to give the virus capsids enough time to traffic to the nucleus. Subsequently, GFP-Mib1 expression was induced with 1 µg/ml doxycycline. After 1 or 3 h, cells were fixed and processed for immunostaining against hexon and click chemistry. Samples were imaged on a Leica SP8 cLSM.

Confocal microscopy

A Leica SP8 cLSM was used in all experiments, in which single viral particles and genomes were imaged. Imaging was performed at a scanning speed of 700 Hz with a 63x magnification oil objective with a numerical aperture of 1.40 and a zoom factor of 2, with a pixel size of 0.181 µm. z-stacks were captured with a step size of 0.5 µm to capture the entire cell, and the size of the pinhole was 1 Airy unit. Leica hybrid detectors (HyD) were used for each channel.

gSTED microscopy

Eighty thousand HeLa-sgNT or HeLa-sgMib1 cells were seeded on cover slips in a 24-well dish. The following day, cells were infected with 4 µg of AdV-C5-atto565. After 3 h, unbound virus was washed away and the cells were incubated in fresh medium for an additional 5 h. Cells were fixed, quenched, and permeabilized and subsequently stained with Mab414 antibody against nuclear pore complexes (1:100 dilution) and goat anti-mouse-Abberior STAR 635P (1:100 dilution). The cover slips were mounted onto ProLong Gold Antifade Mountant (Thermo Fisher Scientific) and imaged the following day on a Leica SP8 inverse STED 3X microscope. Images were acquired with a 100x, 1.40NA objective with a pixel size of 14 nm and gating from 1.5 to 6 ns. A 660 nm depletion laser was used for the atto565 fluorophore, a 775 nm depletion laser was used for Abberior STAR 635P. Due to slight drift during image acquisition, CellProfiler was used to align STED images from each channel to their respective confocal images, which were taken without STED mode at the beginning of the image sequence.

Confocal spinning-disc live microscopy

Eight thousand HeLa-sgMib1 cells transduced with a doxycycline-inducible GFP-Mib1 lentivirus were seeded in a 10-well CELLview slide (Greiner Bio-One) with a 175 µm thick cover glass embedded in its bottom. After two days, the cells were incubated with AdV-C5-atto565 for 30 min at 37°C, or left uninfected. Unbound virus was washed away and the cells were incubated for another 60 min at 37°C so that most viral capsids would reach the nuclear envelope. Fresh medium without phenol-red containing 1 µg/ml doxycycline was added to the cells to induce expression of GFP-Mib1, and live imaging was started 1 h later on a Visitron CSU-W1 spinning disk microscope consisting of a Nikon Eclipse T1 microscope and a Yokogawa confocal scanning unit W1 with a stage top incubation system at 37°C and 5% CO_2. Z-stacks consisting of four steps with a step size of 1.4 µm were acquired every 30 s for ca. 120 min with a 100x oil objective (NA 1.4) and a pinhole of 50 µm. The focus was maintained with a perfect focus system (PFS).

Transmission electron microscopy

About $2.5x10^6$ HeLa-sgNT or HeLa-sgMib1 cells were seeded in 10 cm dishes. The next day, they were infected with 325 µg wt AdV-C5. After 1h at 37°C, the virus inoculum was

removed and the cells were fixed after 0, 1, 4, or 6 Mib1 of further incubation at 37°C. For fixation, cells were washed once with PBS-Ca^{2+}/Mg^{2+}(PBS supplemented with 0.5 mM $MgCl_2$ and 1 mM $CaCl_2$) and then scraped off into 5 ml PBS-Ca^{2+}/Mg^{2+}. Cells were pelleted by centrifugation at 500 x g for 4 min and resuspended in 750 µl of PBS-Ca^{2+}/Mg^{2+}. 750 µl of fixative (4% glutaraldehyde in PBS-Ca^{2+}/Mg^{2+}) was then added to a final concentration of 2% glutaraldehyde. Cells were incubated for 30 min at RT under rotation, then pelleted (1200 xg for 5 min) and resuspended in 1 ml PBS-Ca^{2+}/Mg^{2+}. Cells were then pelleted and resuspended in 400 µl 2% agar noble (BD Biosciences) solution in PBS-Ca^{2+}/Mg^{2+} and placed at 65°C for 5 min. Cells were centrifuged in a swing rotor at 3000 xg for 5 min, yielding a cell pellet in solidified agar while the rest of the agar was discarded. The cell pellet was then incubated in a 1% reduced osmium tetroxide solution (freshly prepared from a 1:1 solution of 2% osmium tetroxide and 3% potassium ferricyanide) for 1 h on ice. Cells were then rinsed three times for 30 min in PBS-Ca^{2+}/Mg^{2+} and 5 min in ddH_2O, then pre-stained with a 2% uranyl acetate solution overnight at 4°C. For sample dehydration, the samples were successively incubated with 30% acetone for 5 min, 50% acetone for 5 min, 70% acetone for 30 min, 90% acetone for 10 min, 100% acetone for 5 min and 100% acetone for 10 min. Samples were embedded in a 48% epoxy resin containing 16% dodecenyl succinic anhydride, 34% methyl nadic anhydride, and 2% benzyldimethylamine. The resin was allowed to polymerize at 60°C for 3 days. Ultrathin 100 nm sections were obtained with a Leica Ultracut UCT ultramicrotome (Leica Microsystems) and mounted on copper grids with parlodion-carbon support film, placed sideways on a droplet of 2% uranyl acetate in H_2O for 30 min, immersed repeatedly in H_2O, dried overnight, placed on a droplet of Sato's lead staining solution for 20 min, washed in H_2O and then dried for 30 min. Samples were imaged in a FEI CM100 electron microscope at 80 kV.

Image analysis

Images were analyzed and quantified by using custom CellProfiler (version 2.1.1) and KNIME (version 2.12.2) pipelines. For infection assays, the nuclei were segmented using the DAPI channel, and the mean GFP intensity on the identified nuclei was measured. The GFP intensity threshold for infection was based on the non-infected controls. For quantification of single viral particles and genomes, maximum projections of the image stacks were used. Nuclei and cell outlines were segmented according to the DAPI and the

succinimidyl ester staining, respectively. In cases where no succinimidyl ester was included, the channel with the strongest cellular background was used for the cell segmentation. Viral particles and/or genomes inside the cell outlines were then segmented and the mean intensities of the other channels on these objects were reported.

QUANTIFICATION AND STATISTICAL ANALYSIS

Unless otherwise indicated, graphs display mean ± standard deviation (SD) and represent data from at least three independent experiments. All data was plotted and statistical analyses performed with GraphPad Prism 8.0 software (GraphPad). Significance indicated by asterisks is designated as follows: *, $p<0.05$; **, $p<0.01$; ***, $p<0.001$; ns, non-significant. The following statistical tests were used: Unpaired (two-tailed) t-test, Figures 1E-F; Ordinary one-way ANOVA with Holm-Sidak correction for multiple comparisons, Figures 1C, 1G, 4B; Mann-Whitney test, Fig. 2B; non-parametric ANOVA (Kruskal-Wallis test) with Dunn's correction for multiple comparisons, Figures 2C, 2D, 2E, 3A, 3C. As indicated in the relevant figures, the term 'n' refers to the number of cells (Figures 2B-E, 3A, supplemental figure 3B,C) or the number of viral particles (Figure 3C) used in the analysis.

DATA AND CODE AVAILABILITY

The data from the genome-wide RNAi screen are in Supplemental Table 1. The results of the gene ontology enrichment analyses are in Supplemental Tables 2 and 3. The code for the various scripts that were used to analyze the images are available by contacting the Lead Author.

KEY RESOURCES TABLE

REAGENT or RESOURCE	SOURCE	IDENTIFIER
Antibodies		
Rabbit polyclonal anti-Adenovirus protein VI	(Burckhardt et al., 2011)	N/A
Anti-Adenovirus antibody (anti-Hexon), Dil: 1:1000	Millipore	Cat# MAB8052, RRID: AB_95243,
Mouse anti-Hexon antibody 9C12	(Varghese et al., 2004)	N/A
Mouse anti-E1A antibody M73, Dil: 1:500	Millipore	Cat# 05-599, RRID: AB_309833
Rabbit monoclonal anti-Mib1 antibody, Dil: 1:1000	Abcam	Cat# ab124929, RRID: AB_11127834
Mouse anti-GAPDH antibody, Dil: 1:2500	Thermo Fisher Scientific	Cat# MA5-15738, RRID: AB_10977387
Mouse monoclonal anti-flag antibody FG4R, Dil: 1:1000	Thermo Fisher Scientific	Cat# MA5-91878, RRID: AB_1957945
Rabbit polyclonal anti-flag antibody, Dil: 1:1000	Sigma-Aldrich	Cat# F7425, RRID: AB_439687
Mouse monoclonal anti-IAV NP antibody HB-65	ATCC, (Yamauchi et al., 2011)	Cat# HB-65, RRID: CVCL_4524
Mouse monoclonal Mab414, Dil: 1:500	Abcam	Cat# ab24609, RRID: AB_448181
Goat anti-Mouse IgG antibody, AlexaFluor 488, Dil: 1:500	Thermo Fisher Scientific	Cat# A-11029, RRID: AB_138404
Goat anti-Mouse IgG antibody, AlexaFluor 594, Dil: 1:500	Thermo Fisher Scientific	Cat# A-11005, RRID: AB_141372
Goat anti-Mouse IgG antibody, AlexaFluor 680, Dil: 1:500	Thermo Fisher Scientific	Cat# A-21058, RRID: AB_2535724

Goat anti-Rabbit IgG antibody, AlexaFluor 488, Dil: 1:500	Thermo Fisher Scientific	Cat# A-11034, RRID: AB_2576217
Goat anti-Rabbit IgG antibody, AlexaFluor 594, Dil: 1:500	Thermo Fisher Scientific	Cat# A-11037, RRID: AB_2534095
Goat anti-Rabbit IgG antibody, AlexaFluor 680, Dil: 1:500	Thermo Fisher Scientific	Cat# A-21109, RRID: AB_2535758
Goat anti-Mouse IgG antibody, HRP-linked, Dil: 1:5000	Cell Signaling	Cat# 7076, RRID: AB_330924
Goat anti-Rabbit IgG antibody, HRP-linked, Dil: 1:5000	Cell Signaling	Cat# 7074, RRID: AB_2099233
Bacterial and Virus Strains		
Competent cells DH5a strain		N/A
AdV-C5 (wt300)	(Hearing and Shenk, 1983)	N/A
AdV-C5-GFP	This paper	N/A
AdV-C5-EdC (genome-labeled)	(Wang et al., 2013)	N/A
AdV-C5-atto565 (capsid-labeled)	(Luisoni et al., 2015)	N/A
AdV-C2-dE3B-CMV-GFP	(Yakimovich et al., 2012)	N/A
AdV-A31	Anja Ehrhardt	N/A
AdV-B3		N/A
AdV-D8		N/A
Influenza A virus x31 (H3N2)	Virapur, (Yamauchi et al., 2011)	N/A
HSV-1-GFP C12	(Glauser et al., 2010)	N/A
VSV-GFP	(Hayer et al., 2010)	N/A
Chemicals, Peptides, and Recombinant Proteins		
DAPI (4',6-diamidino-2-phenylindole)	Sigma-Aldrich	Cat# D9542

Lipofectamine RNAiMAX	Thermo Fisher Scientific	Cat# 13778075
Alexa Fluor 647 NHS Ester (Succinimidyl Ester)	Thermo Fisher Scientific	Cat# A37566
Alexa Fluor 488 Azide, Triethylammonium Salt	Thermo Fisher Scientific	Cat# A10266
Alexa Fluor 594 Azide, Triethylammonium Salt	Thermo Fisher Scientific	Cat# A10270
THPTA (Tris(3-hydroxypropyltriazolylmethyl)amine)	Sigma-Aldrich	Cat# 762342
AG (Aminoguanidine hydrochloride)	Sigma-Aldrich	Cat# 396494
Copper sulfate	Sigma-Aldrich	Cat# 61230
(+)-Sodium L-ascorbate	Sigma-Aldrich	Cat# 11140
Doxycycline	Clontech	Cat# 631311
ECL Prime Western Blotting Detection Reagent	Amersham	Cat# RPN2232
Critical Commercial Assays		
Zyppy Plasmid Miniprep Kit	Zymo Research	Cat# D4036
NucleoBond Xtra Midi Kit	Macherey Nagel	Cat# 740410.100
Experimental Models: Cell Lines		
HeLa	ATCC	CCL-2, RRID: CVCL_0030
HEK293T	ATCC	CRL-3216, RRID: CVCL_0063
A549	ATCC	CCL-185, RRID: CVCL_0023
WI-38	ATCC	CCL-75, RRID: CVCL_0579
Oligonucleotides		
See Supplemental Table S4		
Recombinant DNA		

lentiCRISPR v2	(Sanjana et al., 2014)	Addgene #52961
eSpCas9(1.1)	(Slaymaker et al., 2016)	Addgene #71814
Lenti-eCas9	This paper	N/A
Lenti-eCas9-sgMib1	This paper	N/A
Lenti-eCas9-sgNT	This paper	N/A
pLVX-IRES-puro	Clontech	Cat# 632183
pLVX-Mib1_res	This paper	N/A
pLVX-flag-Mib1	This paper	N/A
pLVX-flag-Mib1-C995S	This paper	N/A
pLVX-flag-Mib1-S805A	This paper	N/A
pLVX-flag-Mib1-1-221	This paper	N/A
pLVX-flag-Mib1-1-818	This paper	N/A
pLVX-flag-Mib1-222-1006	This paper	N/A
pLVX-flag-Mib1-222-818	This paper	N/A
pCW57.1	David Root	Addgene #41393
pLVX-tet-BSD	This paper	N/A
pEGFP-C1	Clontech	Cat# 6084-1
pEGFP-Mib1	This paper	N/A
pLVX-tet-BSD-EGFP-Mib1	This paper	N/A
pCMV-dR8.91-Gag-Pol	Jovan Pavlovic (Crameri et al., 2018)	N/A
pVSV-G	Clontech	Cat# 631530
p3HA-hMib1	Vanessa Redecke	Addgene #33317
Software and Algorithms		
GraphPad Prism version 8.0	GraphPad Software	https://Mib1.graphpad.com/
Fiji	(Schindelin et al., 2012)	https://fiji.sc/#download

Leica Application Suite LAS	Leica	https://Mib1.leica-microsystems.com/products/microscope-software/p/leica-las-x-ls/
CellProfiler version 2.1.1	(Carpenter et al., 2006)	https://cellprofiler.org/releases/
KNIME version 2.12.2	KNIME	https://Mib1.knime.com/downloads

Supplemental Items

Supplemental Tables

Supplemental Table 1: Infection indices and cell numbers of the genome-wide RNAi screen including Z-scores of HeLa cells infected with AdV-C2-ΔE3B_GFP (related to Fig. 1).

Table shows the gene identifiers, the gene names, the Z-scores for the infection indices and for the cell number for each replicate (rG1, rG2), and the averages of the two measurements.

Supplemental Table 2: Gene ontology enrichment analysis of the top 500 infection reducing hits (related to Fig. 1).

Gene ontology (GO) enrichment analysis of the 500 candidates with the lowest infection Z-scores from Supplemental Table 1 using the “cellular components enrichment” tool of the STRING database. The genes identified for each GO term are listed with their Ensembl protein identifiers and their gene names.

Supplemental Table 3: Gene ontology enrichment analysis of the top 500 infection enhancing hits (related to Fig. 1).

Gene ontology (GO) enrichment analysis of the 500 candidates with the highest infection Z-scores from Supplemental Table 1 using the “cellular components enrichment” tool of the STRING database.

Supplemental Table 4: List of oligonucleotides (related to STAR Methods).

Supplemental Movies

Supplemental Movie 1: Transient colocalization of GFP-Mib1 with NPC-docked fluorescent AdV-C5 increases the motility of the virions (related to Fig. 4).

HeLa-sgMib1 cells containing a GFP-Mib1 cassette under a tetracycline-response element were incubated with atto565-labeled AdV-C5 for 90 min. Expression of GFP-Mib1 was then induced with 1 µg/ml doxycycline, and cells were imaged in a confocal spinning-disk microscope starting at 1 h post induction. Four z-slices were imaged at an interval of 30 s, of which one slice is shown. Green, GFP-Mib1; magenta, AdV-C5. Arrows indicate events of colocalization at the nuclear envelope. Time stamps indicate h:min:sec. Scale bar, 10 µm.

Supplemental Movie 2: Localization and movement of Mib1 puncta in non-infected cells (related to Fig. 4).

HeLa-sgMib1 cells containing a GFP-Mib1 gene expression cassette under a tetracycline-response element were treated and imaged as in Supplemental Movie, except that they were not infected by AdV. There was no apparent difference in the localization or movement of the GFP-Mib1 puncta compared to the infected cells.

F1

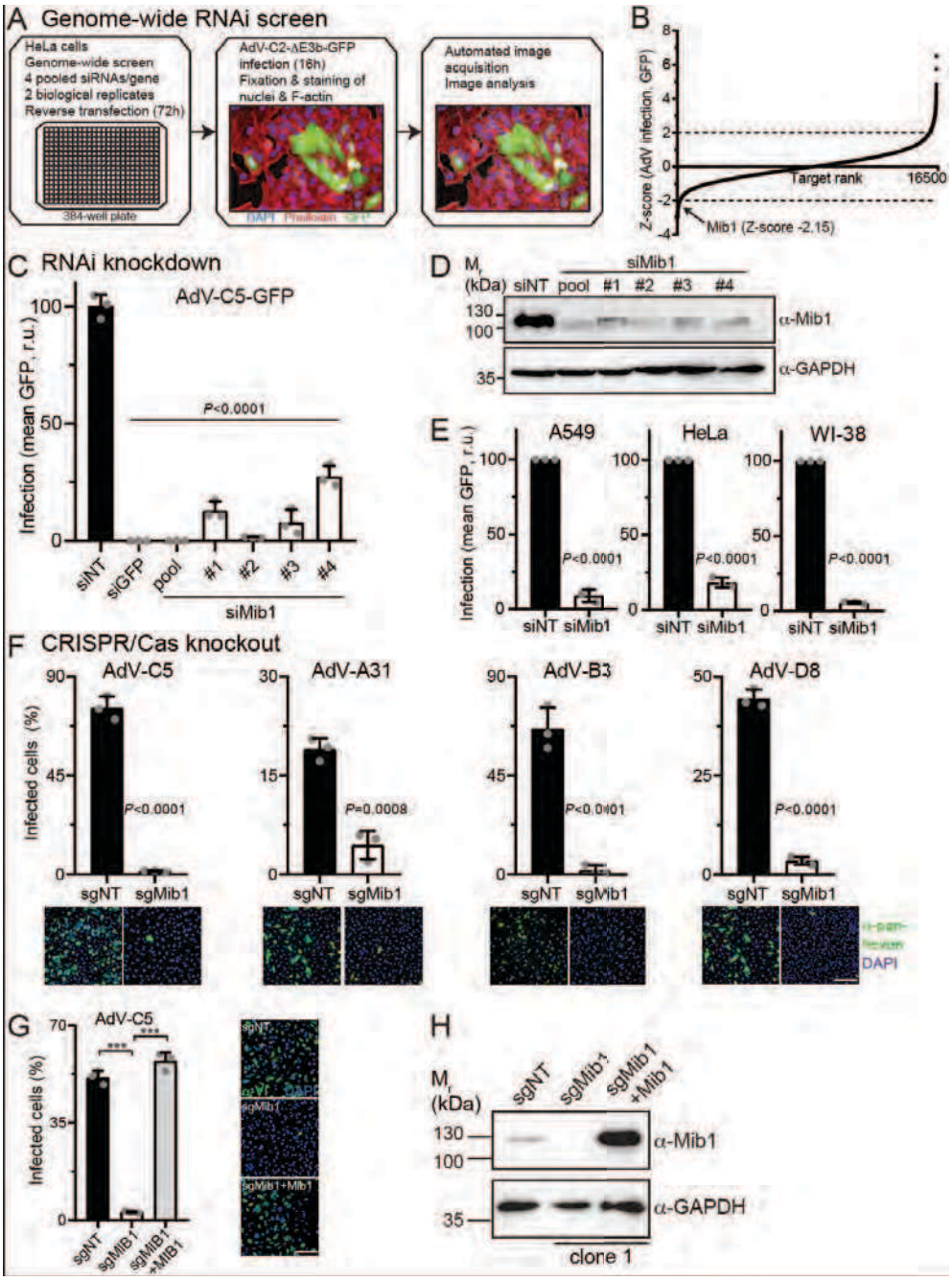
A Genome-wide RNAi screen
HeLa cells
Genome-wide screen
4 pooled siRNAs/gene
2 biological replicates
Reverse transfection (72h)
384-well plate
AdV-C2-ΔE3b-GFP
infection (16h)
Fixation & staining of
nuclei & F-actin
Automated image
acquisition
Image analysis
B
Z-score (AdV infection, GFP)
Target rank
16500
Mib1 (Z-score -2.15)
C RNAi knockdown
AdV-C5-GFP
Infection (mean GFP, r.u.)
P<0.0001
siNT
siGFP
pool
#1
#2
#3
#4
siMib1
D
M, (kDa)
siNT
pool
siMib1
#1
#2
#3
#4
130
100
35
α-Mib1
α-GAPDH
E
A549
HeLa
WI-38
Infection (mean GFP, r.u.)
P<0.0001
siNT
siMib1
F CRISPR/Cas knockout
AdV-C5
AdV-A31
AdV-B3
AdV-D8
Infected cells (%)
P<0.0001
P=0.0008
sgNT
sgMib1
DAPI
G
AdV-C5
Infected cells (%)
***
sgNT
sgMIB1
sgMIB1 +MIB1
H
M, (kDa)
sgNT
sgMib1
sgMib1 +Mib1
130
100
35
α-Mib1
α-GAPDH
clone 1

F2

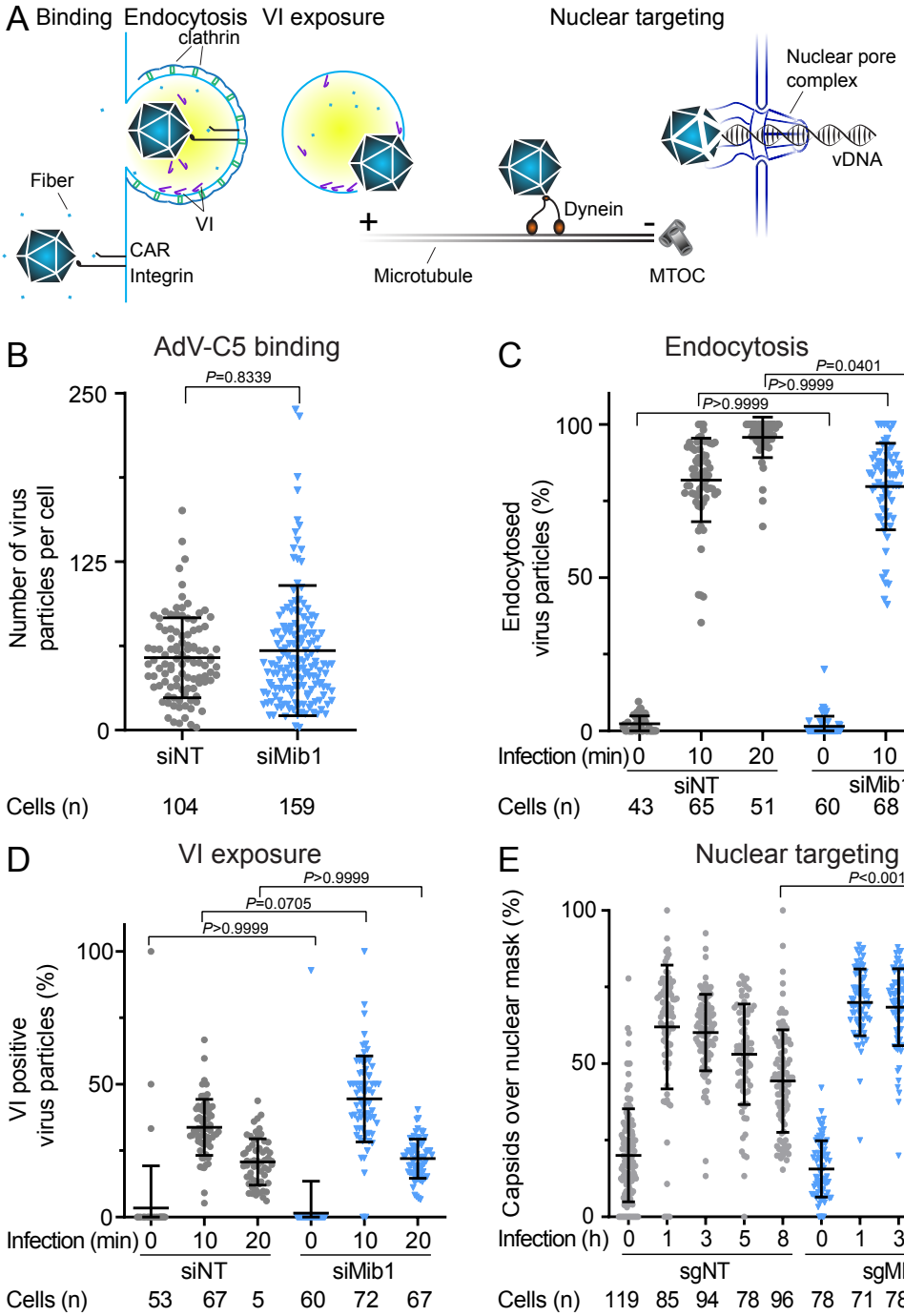
A
Binding
Endocytosis
VI exposure
Nuclear targeting
clathrin
Fiber
VI
CAR
Integrin
Microtubule
Dynein
MTOC
Nuclear pore complex
vDNA
B
AdV-C5 binding
P=0.8339
Number of virus particles per cell
250
125
0
siNT
siMib1
Cells (n)
104
159
C
Endocytosis
P=0.0401
P>0.9999
P>0.9999
Endocytosed virus particles (%)
100
50
0
Infection (min)
0
10
20
0
10
20
siNT
siMib1
Cells (n)
43
65
51
60
68
68
D
VI exposure
P>0.9999
P=0.0705
P>0.9999
VI positive virus particles (%)
100
50
0
Infection (min)
0
10
20
0
10
20
siNT
siMib1
Cells (n)
53
67
5
60
72
67
E
Nuclear targeting
P<0.001
Capsids over nuclear mask (%)
100
50
0
Infection (h)
0
1
3
5
8
0
1
3
5
8
sgNT
sgMIB1
Cells (n)
119
85
94
78
96
78
71
78
76
107

F3

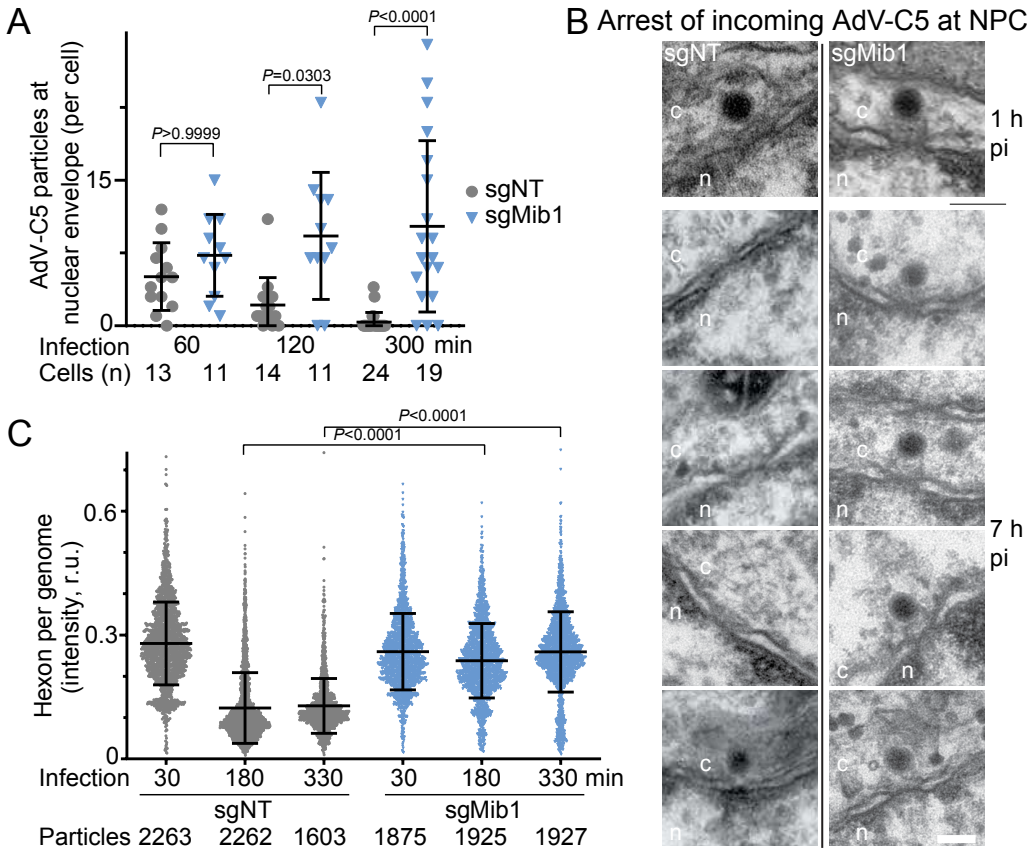
A
AdV-C5 particles at nuclear envelope (per cell)
15
0
P>0.9999
P=0.0303
P<0.0001
sgNT
sgMib1
Infection 60 120 300 min
Cells (n) 13 11 14 11 24 19
B Arrest of incoming AdV-C5 at NPC
sgNT
sgMib1
1 h pi
7 h pi
c
n
C
P<0.0001
P<0.0001
Hexon per genome (intensity, r.u.)
0.6
0.3
0
Infection 30 180 330 30 180 330 min
sgNT
sgMib1
Particles 2263 2262 1603 1875 1925 1927

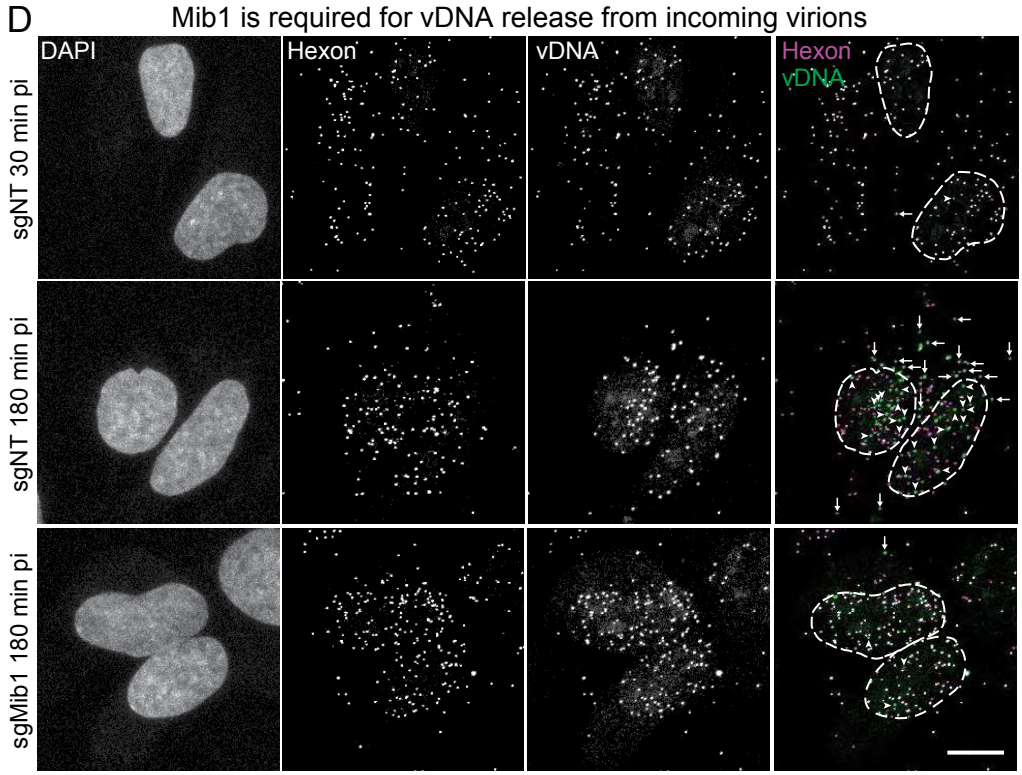
D
Mib1 is required for vDNA release from incoming virions
DAPI
Hexon
vDNA
Hexon
vDNA
sgNT 30 min pi
sgNT 180 min pi
sgMib1 180 min pi

F4

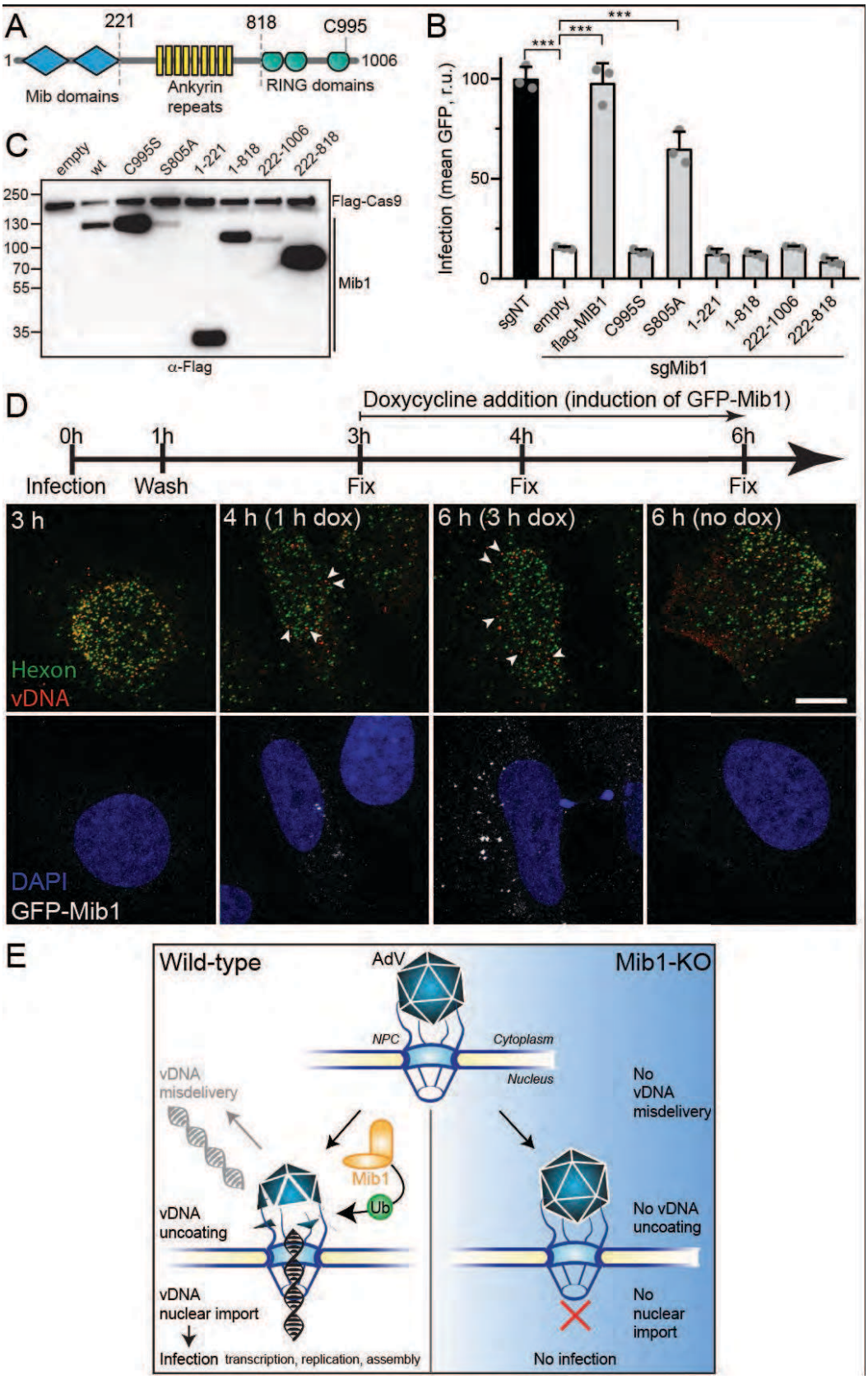
A
221
818
C995
1
1006
Mib domains
Ankyrin repeats
RING domains
B
***
***
***
Infection (mean GFP, r.u.)
100
50
0
sgNT
empty
flag-MIB1
C995S
S805A
1-221
1-818
222-1006
222-818
sgMib1
C
empty
wt
C995S
S805A
1-221
1-818
222-1006
222-818
250
130
100
70
55
35
Flag-Cas9
Mib1
α-Flag
D
Doxycycline addition (induction of GFP-Mib1)
0h
1h
3h
4h
6h
Infection
Wash
Fix
Fix
Fix
3 h
4 h (1 h dox)
6 h (3 h dox)
6 h (no dox)
Hexon
vDNA
DAPI
GFP-Mib1
E
Wild-type
AdV
Mib1-KO
NPC
Cytoplasm
Nucleus
vDNA misdelivery
No vDNA misdelivery
Mib1
Ub
vDNA uncoating
No vDNA uncoating
vDNA nuclear import
No nuclear import
Infection transcription, replication, assembly
No infection

SUPPLEMENTAL MATERIALS

The E3 Ubiquitin Ligase Mind Bomb 1 Controls Adenovirus Genome Release at the Nuclear Pore Complex

M. Bauer, J.W. Flatt, D. Seiler, B. Cardel, M. Emmenlauer, K. Boucke, M. Suomalainen, S. Hemmi & U.F. Greber

Supplemental Figures

SF1

A Sums of gene counts & false discovery rate of the top 500 infection reducing siRNA hits

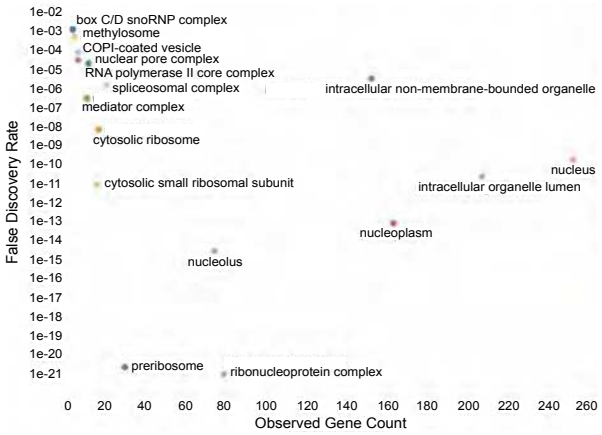

B Sums of gene counts & false discovery rate of the top 500 infection enhancing siRNA hits

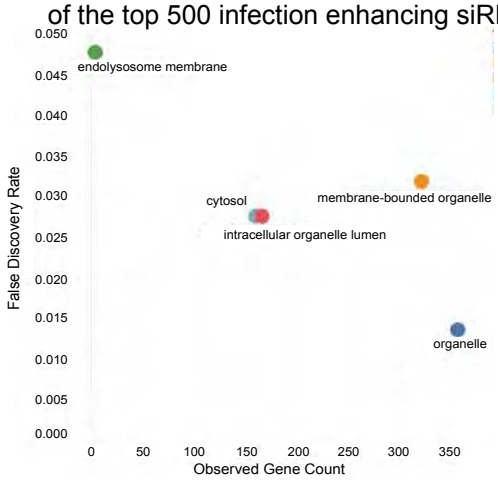

C CRISPR/Cas knockout populations

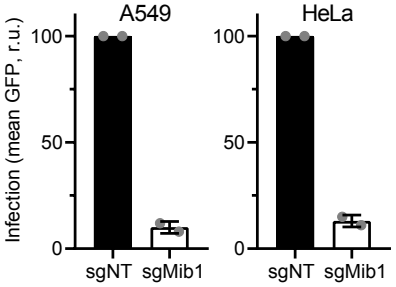

D Western blot

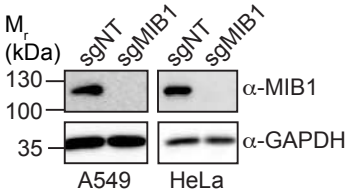

E HeLa-sgMib1 (clone 1)

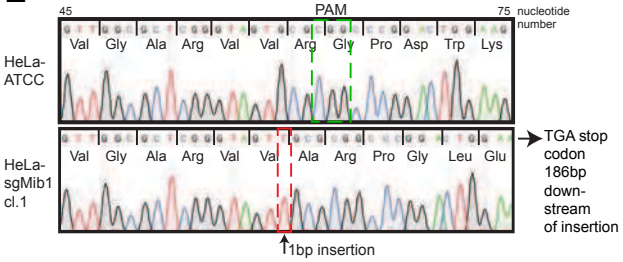

F

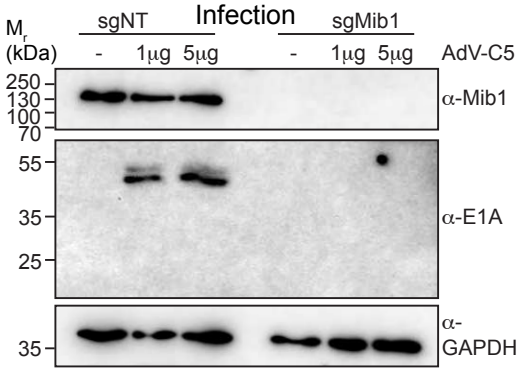

G Mib1 is not required for HSV-1, Lenti, VSV & IAV infections

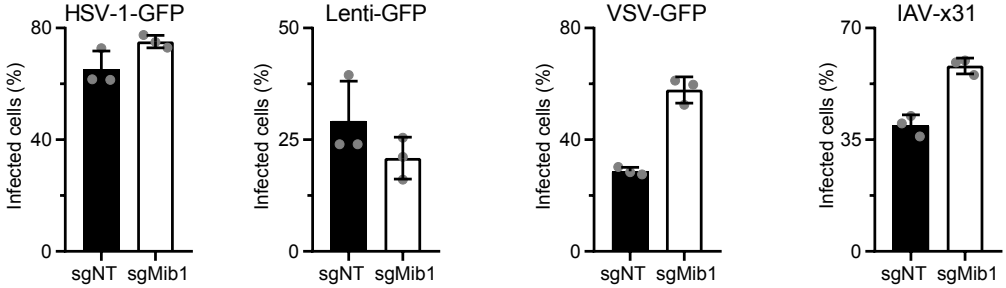

Supplemental Fig. 1: Aggregated hits from the genome wide siRNA screen down- or up-regulating AdV infection and characterization of the CRISPR/Cas9 Mib1 KO cells (related to Fig. 1).

(A) Gene ontology enrichment analysis was performed on the top 500 infection reducing siRNA hits using the “cellular components enrichment” tool of the STRING database.

(B) Gene ontology enrichment analysis was performed on the top 500 infection enhancing siRNA hits as in Supplemental Fig. 1A.

(C) A549 or HeLa cells were transduced with Lenti-eCas9-sgNT or Lenti-eCas9-sgMib1 at a MOI of 0.4. After two days, cells were selected for five days with 2 µg/ml puromycin. The polyclonal puromycin-resistant cell populations were then seeded in a 96-well plate and infected with AdV-C5-GFP for 24 h, after which cells were fixed and nuclei stained with DAPI. Cells were analyzed by fluorescence microscopy, and infection was quantified based on the GFP signal, normalized to the mean GFP signal in the sgNT control cells. Bar graphs show mean ± s.d. from n = 2 independent experiments.

(D) The polyclonal populations described in Supplemental Fig. 1C were lysed and proteins were separated on an SDS-PAGE gel, followed by Western blotting. The membrane was probed with anti-Mib1 and anti-GAPDH antibodies.

(E) Genomic DNA was isolated from HeLa-ATCC cells or from monoclonal HeLa-sgMib1 cells (cl. 1). A 300 bp region containing the Mib1 sequence targeted by the guide RNA was amplified by PCR and cloned into the pBluescript vector, which was then used to transform bacteria. Plasmid DNA from more than 25 clones was isolated and sequenced using the Sanger method. All alleles carried the insertion of a single thymidine after Cas9-sgMib1 treatment, as shown here. PAM (protospacer adjacent motif) of the gRNA is indicated. The Cas9 cuts three bp upstream of the PAM, which is where the extra thymidine was inserted upon DNA repair.

(F) HeLa-sgNT or HeLa-sgMib1 cells were seeded in a 24-well plate and infected with 1 or 5 µg of AdV-C5. At 6 h pi, cells were lysed, and proteins were separated via SDS-PAGE, followed by Western blotting. Membranes were probed with the indicated antibodies.

(G) HeLa-sgNT or HeLa-sgMib1 cells were seeded in a 96-well plate and infected with GFP expressing HSV-1 (HSV-1-GFP), VSV-G pseudotyped lentivirus (Lenti-GFP), vesicular stomatitis virus (VSV-GFP). A549-sgNT and A549-sgMib1 cells were infected with the H3N2 influenza A virus strain x31 (IAV x31). All cells were fixed at 7 h pi, except for Lenti-GFP infected cells which were fixed at 24 h pi. IAV infection was visualized by immunostaining with anti-NP antibody (HB-65). Nuclei were stained with DAPI and cells were imaged by fluorescence microscopy. Infection was scored by percentage of protein GFP-positive nuclei or HB-65-positive nuclei in the case of IAV. Data from n = 3 independent experiments is shown. All bar graphs in this figure depict mean ± s.d.

SF2

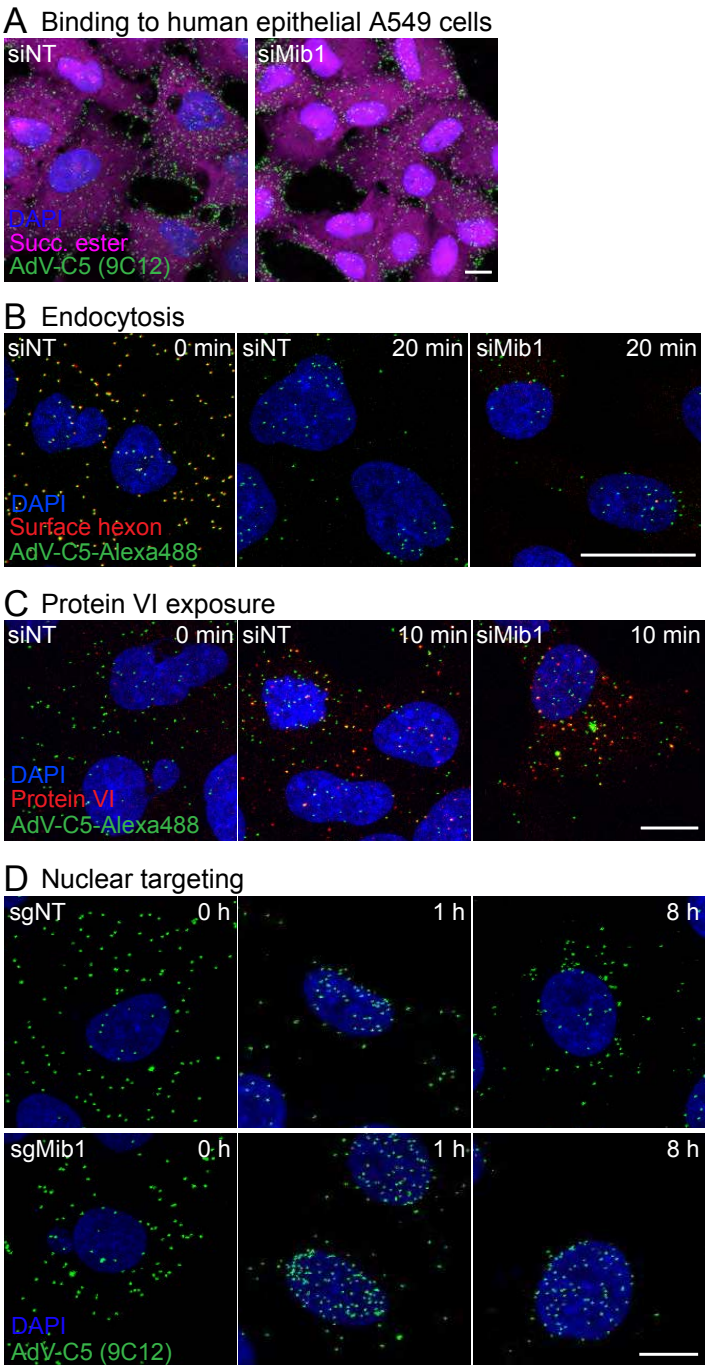

Supplemental Fig. 2: Fluorescence micrographs underlying analyses of AdV cell binding, endocytosis, exposure of the membrane-lytic protein VI and virion nuclear targeting (related to Fig. 2).

(A-D) show representative maximum projection images of A549 cells corresponding to the Fig. 2 (B-E). Scale bars, 10 µm.

SF3

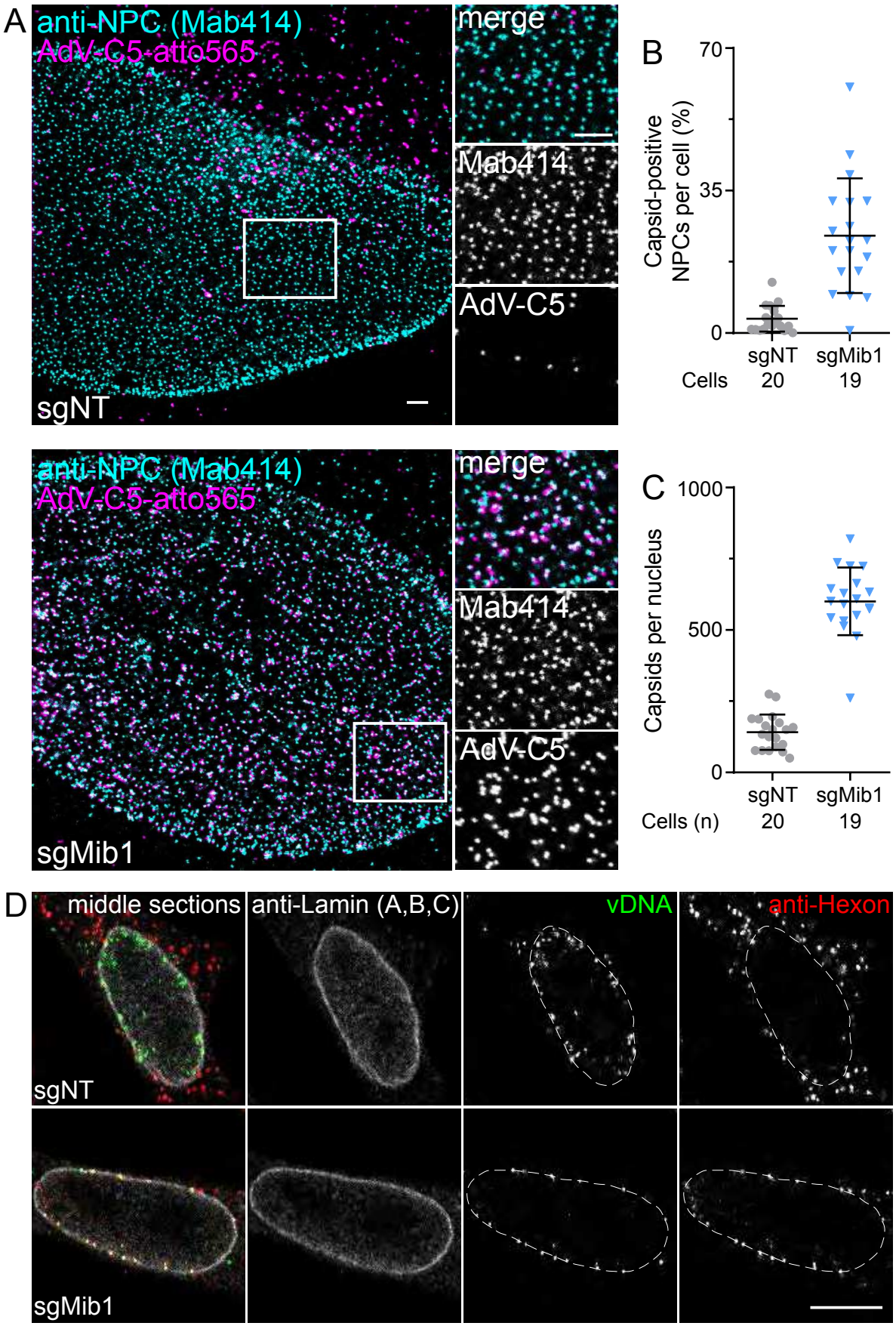
A
anti-NPC (Mab414)
AdV-C5-atto565
merge
Mab414
AdV-C5
sgNT
sgMib1
B
Capsid-positive NPCs per cell (%)
70
35
0
sgNT
sgMib1
Cells
20
19
C
Capsids per nucleus
1000
500
0
sgNT
sgMib1
Cells (n)
20
19
D
middle sections
anti-Lamin (A,B,C)
vDNA
anti-Hexon
sgNT
sgMib1

Supplemental Fig. 3: Enhanced colocalization of incoming AdV with the NPCs in Mib1 KO cells (related to Fig. 3).

(A) HeLa-sgNT and HeLa-sgMib1 cells were seeded on cover slips in a 24-well plate.

The following day cells were incubated with atto565-labeled AdV-C5. After 3 h at 37°C, unbound virus was washed away and cells were incubated for another 5 h, after which cells were fixed. Nuclear pore complexes were stained with the Mab414 antibody. Cells were imaged with a confocal gSTED super-resolution microscope. The images show the bottom of the nuclear membrane. Significantly more virus capsids are docked at NPCs in the sgMib1 cells than the control cells. Scale bars, 1 µm.

(B) The NPCs were segmented and probed for AdV signal. Colocalization was assessed by thresholding of the AdV-atto565 intensity over each NPC.

(C) AdV particles over the nuclear membrane were segmented and counted in each image.

(D) HeLa-sgNT and HeLa-sgMib1 cells were infected with AdV-C5-EdC for 5 h, fixed, and stained for hexon, vDNA, and lamin. Image stacks were acquired across the entire nucleus. To distinguish nuclear from cytoplasmic vDNA, we analyzed single optical sections across the center of the nuclei where hexon was outside the nucleus. In sgNT cells, capsid-free vDNA can be seen inside the nucleus, whereas in sgMib1 cells most of the vDNA puncta colocalize with hexon at the nuclear membrane. Scale bar, 10 µm.

SF4

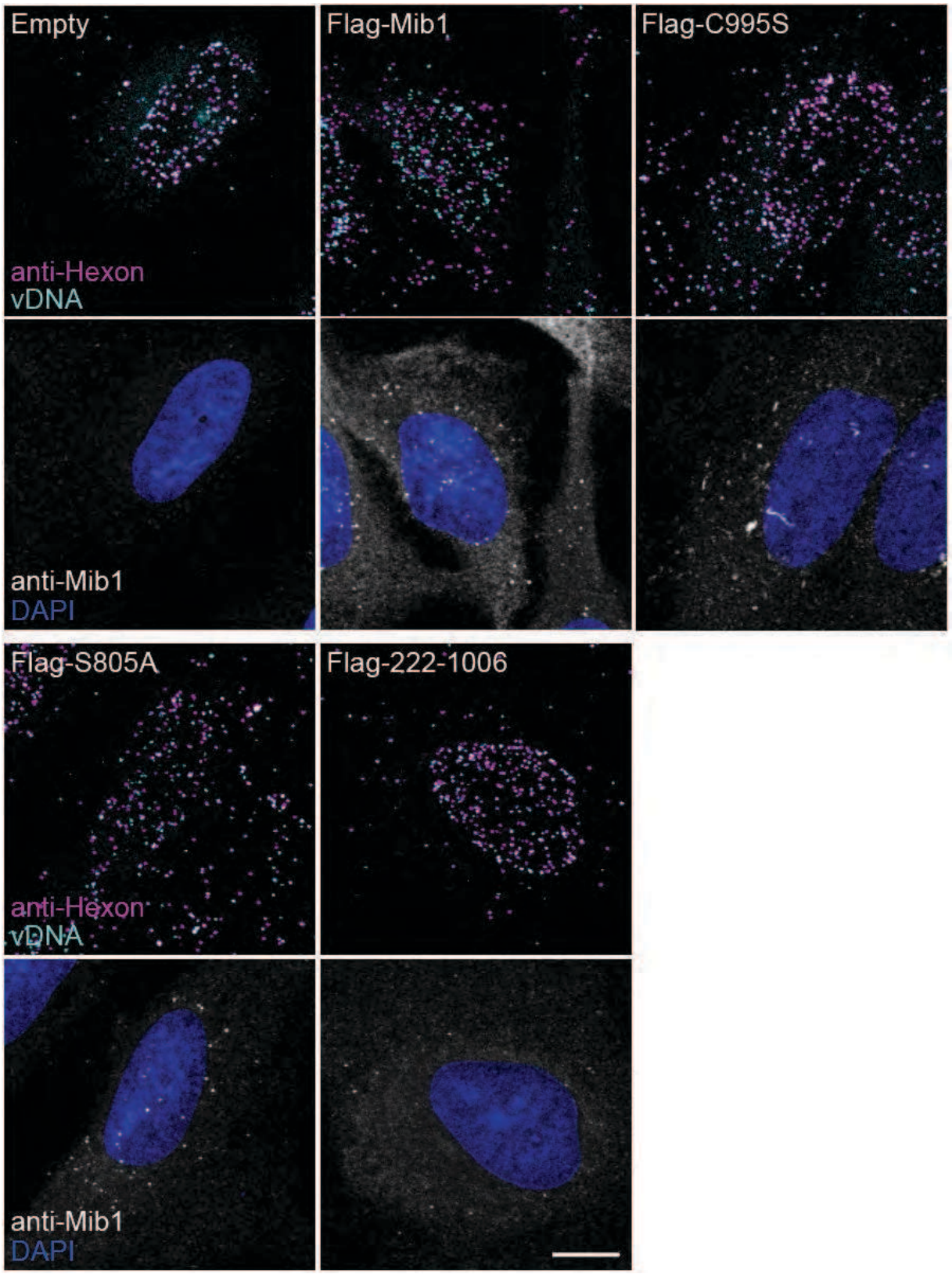
Empty
Flag-Mib1
Flag-C995S
anti-Hexon
vDNA
anti-Mib1
DAPI
Flag-S805A
Flag-222-1006
anti-Hexon
vDNA
anti-Mib1
DAPI

Supplemental Fig. 4: Single cell, single genome analyses of AdV DNA uncoating in sgMib1 cells expressing flag-tagged Mib1 constructs (related to Fig. 4).

HeLa-sgMib1 cells were transduced with lentivirus for expression of the indicated constructs. After two days, cells were incubated with AdV-C5-EdC for 1 h on ice, after which unbound virus was washed away and infection was allowed to progress for 3 h. Cells were then fixed with 4% PFA and processed for immunostaining with anti-hexon and anti-Mib1 antibody, followed by click chemistry for incoming viral DNA and DAPI for nuclei. Cells were imaged with a confocal microscope. Genome release was only observed in cells expressing wild-type Mib1 or the S805A mutant. Shown are maximum projections of representative images. Scale bar, 10 µm.

Supplemental Table 4: List of oligonucleotides (related to STAR Methods).

Oligonucleotide name	Sequence	Purpose
siMib1 #1	Dharmacon, GACCUGAGCAUUCGAAAUA	RNAi
siMib1 #2	Dharmacon, GGUAUGCUCUGACAAGAAA	RNAi
siMib1 #3	Dharmacon, GUAAGAAACGUGAUGAUAU	RNAi
siMib1 #4	Dharmacon, CGAAGAGUGCCUUUCAUUA	RNAi
siNT (non-targeting)	Dharmacon, Cat# D-001810-01-05	RNAi
sgMib1_f	caccGTTGGCGCTCGGGTAGTGCG	CRISPR
sgMib1_r	aaacCGCACTACCCGAGCGCCAAC	CRISPR
sgNT_f	caccgACGGAGGCTAAGCGTCGCAA	CRISPR
sgNT_r	aaacTTGCGACGCTTAGCCTCCGTc	CRISPR
Mib1_EcoRI_f	TAAGCAGAATTCATGAGTAACTCCCGGAATAACC	Cloning
Mib1_NotI_r	TGCTTAGCGGCCGCGGAATTCGCCCTTTCTTTAC	Cloning
Mib1_XhoI_f	TTGCTCCTCGAGCTATGAGTAACTCCCGGAATAAC	Cloning
Mib1_EcoRI_r	TGGCAAGAATTCGGAATTCGCCCTTTCTTTAC	Cloning
Mib1_res_f	agttgtcagaGGCCCGGACTGGAAGTGG	Mutagenesis
Mib1_res_r	cttgcccctacCCCTTCCACCATCACCCG	Mutagenesis
3xFLAG-Mib1_f	cgattacaaggatgacgatgacaagggtggaggcggttccAGTAACTCCCGGAATAAC	Mutagenesis
3xFLAG-Mib1_r	atgtcatgatctttataatcaccgtcatggtctttgtagtcCATGAATTCACCGGAAATAG	Mutagenesis
Mib1_C995S_f	TGTCCTATCTcTCGCAAGGCTATTG	Mutagenesis
Mib1_C995S_r	TTCACTCATGCGGTCTCC	Mutagenesis
Mib1_S805A_f	GGGTTCTCGGgcTCCTTCTATGATTAGTAATG	Mutagenesis
Mib1_S805A_r	ACTTGACCACTGACTTTTTC	Mutagenesis
Mib1_1-221_f	TAAAGTAAAGAAAGGGCTAATTC	Mutagenesis

Mib1_1-221_r	GGCATCCTGGACACATTTC	Mutagenesis
Mib1_1-818_r	CTCTTCTAAGGTTTCAGAATC	Mutagenesis
Mib1_222-1006_f	AAGGGAGGTTCTTTCTACAGAGATC	Mutagenesis
Mib1_222-1006_r	GGAACCGCCTCCACCCTT	Mutagenesis
M13r	CAGGAAACAGCTATGACC	Sequencing
Mib1_seq	AGCTGTGCCGTTGTCCCACA	Sequencing